PIM kinase control of CD8 T cell protein synthesis and cell trafficking

Julia M Marchingo[1,3,#], Laura Spinelli[1,2], Shalini Pathak[1,4], Doreen A Cantrell[1,#]

Affiliations:

1. Cell Signalling and Immunology Division, School of Life Sciences, University of Dundee, United Kingdom
2. Molecular Cell and Developmental Biology Division, School of Life Sciences, University of Dundee, United Kingdom
3. Current address: Blood Cells and Blood Cancer Division, Walter and Eliza Hall Institute of Medical Research, Melbourne, Australia
4. Current address: Innovation Factory Core Technology Facility, University of Manchester, UK

Correspondence: d.a.cantrell@dundee.ac.uk (D.A.C.), marchingo@wehi.edu.au (J.M.M.)

Abstract:

Integration of a large network of kinase signalling pathways co-ordinates changes in the transcription, translation and metabolic events required for T cell activation and differentiation. The present study explores the role of the Serine/Threonine kinases PIM1 and PIM2 in controlling murine CD8 T lymphocyte antigen receptor-mediated activation and differentiation in response to the cytokines Interleukin 2 (IL-2) or IL-15. We show that PIM kinases are dispensable for the differentiation programs controlled by the antigen-receptor and IL-15. There is however a selective role for the PIM kinases in the context of IL-2 regulation of CD8 T cell fate. One key insight was that the PIM kinases controlled the migratory capabilities of effector CD8 T cells, with *Pim1*/*Pim2*-deficient CD8 T cells unable to fully switch off the naïve T cell chemokine and adhesion receptor program during effector differentiation. PIM kinases were also needed for IL-2 to sustain high expression of the glucose transporters SLC2A1 and SLC2A3 and to maintain activity of the nutrient sensing kinase mTORc1. Strikingly, PIM kinases did not have a dominant impact on IL-2-driven transcriptional programs but rather selectively modulated protein synthesis to shape cytotoxic T cell proteomes. This study reveals a selective role of PIM kinases in IL-2 control

32 of CD8 T cells and highlights how regulated changes in protein synthesis can impact T cell
33 phenotypes.

34 **Introduction:**

35 CD8 T lymphocytes are key effector cells for adaptive immune responses to viruses,
36 intracellular pathogens and tumours. Their clonal expansion and differentiation to cytotoxic
37 effector or memory CD8 T cells is controlled by signalling pathways initiated by the T cell
38 antigen receptor (TCR), co-stimulatory molecules and cytokines. Receptor engagement by
39 immune stimuli triggers the activation of cytosolic tyrosine kinases that then direct the
40 activity of a diverse network of Serine/Threonine kinases, disseminating signals from plasma
41 membrane to cell interior. The Src family and ZAP70 Tyrosine kinases initiate this process
42 downstream of the TCR, with the Janus kinases (JAK) as the main signal transducer for
43 important cytokine regulators of T cell differentiation, IL-2 and IL-15 (Cantrell, 2015; Saravia
44 et al., 2020). The subsequent network of Serine/Threonine kinases that is engaged beyond
45 these initiating events coordinates phosphorylation of a diverse array of protein targets.
46 These protein targets include chromatin regulators, transcription factors, translation
47 machinery, cytoskeletal proteins and metabolic enzymes, which then control the changes in
48 transcriptional, translational and metabolic programs that drive effector and memory T cell
49 differentiation (Navarro et al., 2011; Tan et al., 2017; Locard-Paulet et al., 2020).
50

51 CD8 T cells express ∼200 Serine/Threonine protein kinases (Navarro et al., 2014; Howden et
52 al., 2019). There is a good understanding of the roles of some Serine/Threonine kinases in
53 CD8 T cells, including the role of the diacylglycerol regulated kinases, MAP kinases ERK1 and
54 2, Phosphatidylinositol (3,4,5) triphosphate- controlled kinases PDK1 and AKT, and the
55 nutrient sensing kinases mammalian Target of Rapamycin complex 1 (mTORc1) and AMP-
56 activated protein kinase (AMPK) (Finlay et al., 2012; Rolf et al., 2013; Blagih et al., 2015;
57 Cantrell, 2015; Hukelmann et al., 2016; Tan et al., 2017; Howden et al., 2019; Saravia et al.,
58 2020; Damasio et al., 2021; Spinelli et al., 2021). However, beyond these core kinases there
59 is much still to learn about how many of the ~200 Serine/Threonine kinases expressed in
60 CD8 T cells contribute to the control of T cell function. In this context, the PIM kinases are a
61 family of Serine/Threonine kinases that are strongly and rapidly induced in T cells
62 responding to immune stimuli (Aho et al., 2005; Fox et al., 2005; Peperzak et al., 2010;
63 Jackson et al., 2012). The PIM family contains 3 Serine/Threonine kinases, PIM1, PIM2 and
64 PIM3, of which T lymphocytes predominantly express PIM1 and PIM2 (Mikkers et al., 2004;
65 Fox et al., 2005). As PIM kinases are constitutively active, their participation in signalling

66 cascades is dictated by regulated changes in their protein expression levels (Warfel and
67 Kraft, 2015). PIM1 and PIM2 have little to no expression in naïve T cells but are induced by
68 T-cell receptor activation and costimulation (e.g. CD27) (Wingett et al., 1996; Fox et al.,
69 2005; Peperzak et al., 2010). PIM kinases are also direct transcriptional targets of JAK/STAT
70 signalling pathways and as such PIM1 and/or PIM2 are rapidly induced in T cells
71 downstream of a diverse array of cytokines, including multiple common cytokine receptor γ-
72 chain family cytokines, IL-6 and IL-12 (Matikainen et al., 1999; Aho et al., 2005; Fox et al.,
73 2005; Warfel and Kraft, 2015; Buchacher et al., 2023).
74
75 There have been some analyses of how deletion of PIM kinases impacts CD8 T cell function.
76 A mild reduction in *Pim1/Pim2/Pim3*-deficient CD4 and CD8 T cell proliferation has been
77 observed in response to sub-optimal TCR stimulation and IL-2 (Mikkers et al., 2004) and
78 there is evidence that PIM1 and PIM2 control survival pathways in naïve CD4 and CD8 T cells
79 in concert with mTORc1 (Fox et al., 2005). *Pim1/Pim2/Pim3* deletion is reported to promote
80 expression of stemness and memory-associated transcription factors including Bcl6 and Tcf7
81 (Chatterjee et al., 2019) and PIM kinase activity has been linked with maintenance of
82 memory CD8 T cell survival (Knudson et al., 2017). It has also been shown recently that
83 *Pim1/Pim2* deficiency prevented mTORc1 activation and the proliferation of non-
84 conventional intra-epithelial gut CD8 T lymphocytes (IEL) in response to the cytokine IL-15
85 (James et al., 2021).
86
87 Elevated PIM kinase expression has been noted in patient T cells for a number of
88 autoimmune conditions, including rheumatoid arthritis, uveitis and coeliac disease, and PIM
89 kinase inhibition has been proposed as a possible intervention to dampen autoimmunity
90 (James et al., 2021; Maney et al., 2021; Li et al., 2022). PIM kinase inhibitors have also
91 entered clinical trials to treat some cancers (e.g. multiple myeloma, acute myeloid
92 leukaemia, prostate cancer), and although they have not been effective as a monotherapy,
93 there is interest in combining these with immunotherapies. This is due to studies showing
94 PIM inhibition reducing expression of inhibitory molecules (e.g. PD-L1) on tumour cells and
95 macrophages in the tumour microenvironment and a reported increase of stem-like
96 properties in PIM-deficient T cells which could potentially drive longer lasting anti-cancer
97 responses (Chatterjee et al., 2019; Xin et al., 2021; Clements and Warfel, 2022). However,

98 PIM kinase inhibition has also generally been shown to be inhibitory for T cell activation,
99 proliferation and effector activities (Fox et al., 2003; Mikkers et al., 2004; Jackson et al.,
100 2012) and use of PIM kinase inhibitors could have the side effect of diminishing the anti-
101 tumour T cell response. Given the role of CD8 T cells in anti-cancer immunity, it is important
102 to understand how these kinases control CD8 T cell function. However, there has not yet
103 been a systematic analysis of the role of PIM kinases in conventional CD8 T cells as they
104 activate and differentiate to form effector and memory cells. Accordingly, the current study,
105 uses high resolution quantitative analysis of *Pim1*/*Pim2*-deficient CD8 T cell proteomes and
106 transcriptomes to obtain a comprehensive and unbiased understanding of how PIM kinases
107 control CD8 T cell TCR-driven activation, and IL-2 or IL-15-driven proliferation, and
108 differentiation. The study reveals a selective role for PIM kinases as mediators of IL-2
109 signalling to control CD8 T cell trafficking and effector functionality. We uncover that the
110 dominant impact of PIM kinase loss was to shape effector CD8 T cell proteomes rather than
111 transcriptomes, reflecting PIM kinase modulation of protein synthesis.
112
113 **Results:**
114 ***PIM1 and PIM2 are strongly induced by antigen receptor engagement but are dispensable***
115 ***for T cell activation***
116 T cell antigen receptor (TCR) -driven activation of naïve T cells initiates their clonal
117 expansion and differentiation into effector and memory cells. Quantitative mass
118 spectrometry-based proteomics analysis of naïve OT1 CD8 T cell stimulated with their
119 cognate peptide over time (Marchingo et al., 2020) showed that PIM1 protein was strongly
120 induced within 3 hours of TCR engagement, which was sustained at a 24 hour time point
121 (**Fig 1A**). PIM2 expression was not detected until 9 hours post-stimulation but was also
122 sustained at the 24-hour time point. 24-hour polyclonal activation of CD8 T cells with
123 αCD3/αCD28 agonist antibodies similarly induced expression of PIM1 and PIM2 proteins
124 (**Fig 1B, Table S1**). These increases in PIM kinases expression at a protein level were
125 underpinned by transcriptional reprograming, with both *Pim1* and P*im2* mRNA very lowly
126 expressed in naïve CD8 T cells and strongly upregulated by immune activation (**Fig 1C**)
127 (Spinelli et al., 2021). Consistent with previous reports of Pim1 and Pim2 being the major
128 PIM kinases in T cells (Mikkers et al., 2004; Fox et al., 2005), *Pim3* mRNA was only expressed

129 at very low levels in naïve and activated CD8 T cells (**Fig 1C**), with PIM3 protein not detected
130 at all by mass spectrometry (**Table S1**).
131
132 PIM1 and PIM2 have similar substrate selectivity and hence functional redundancy (Mikkers
133 et al., 2004; Bullock et al., 2005; Fox et al., 2005; Peng et al., 2007; Warfel and Kraft, 2015).
134 Accordingly, to explore the role of the PIM kinases in T cells, mice with a whole body
135 deletion of *Pim1* and *Pim2*, Pim1$^{-/-}$ (Pim1 KO) (Laird et al., 1993) and Pim2$^{-/-}$ or Pim2$^{-/Y}$ (Pim2
136 KO) (Mikkers et al., 2004), were backcrossed for >10 generations onto a C57BL/6
137 background and inter-crossed to generate *Pim1*/*Pim2* double knockout (Pim dKO) mice.
138 There were normal proportions of peripheral T cells in spleens of Pim dKO mice (**Fig S1A**)
139 similar to what has been reported previously in Pim dKO mice on an FVB/N genetic
140 background (Mikkers et al., 2004), though the total number of T cells and splenocytes was
141 lower than in age/sex matched wild-type (WT) mouse spleens (**Fig S1B-C**). This was not
142 attributable to any one cell type (**Fig S1A)**(James et al., 2021) but was instead likely the
143 result of these mice being smaller in size, a phenotype that has previously been reported in
144 *Pim1/2/3* triple KO mice (Mikkers et al., 2004).
145 We tested how Pim dKO T cells respond to immune activation and observed a normal
146 increase in cell size in response to *in vitro* immune activation with αCD3/αCD28 agonist
147 antibodies (**Fig 1D**). 24-hour αCD3/αCD28 activated Pim dKO CD4 and CD8 T cells also
148 normally upregulated expression of established markers of T cell activation including CD25,
149 CD44 and the transferrin receptor CD71 (**Fig 1E**). 24-hour TCR-activated Pim dKO CD8 T cells
150 also produced normal levels of the key effector cytokine IFNγ (**Fig 1E**) and there was no
151 discernible difference in TCR-driven proliferation between WT and Pim dKO T cells over 3
152 days in culture (**Fig 1F, J**). To systematically explore in an unbiased way if *Pim1*/*Pim2*-
153 deficiency impacted TCR-driven activation phenotypes, we performed high-resolution mass
154 spectrometry to measure the proteomes of 24 hour αCD3/αCD28 activated WT and Pim
155 dKO CD4 and CD8 T cells. Proteomics analysis confirmed that no catalytically active PIM1
156 and PIM2 protein were made in Pim dKO mice (**Fig S2**). These experiments quantified
157 expression of >7000 proteins but found no substantial quantitative or qualitative differences
158 in protein content or proteome composition in activated WT versus Pim dKO CD4 and CD8 T
159 cells (**Fig 1G-H**) (**Table S1**). Collectively these results indicate that PIM kinases do not play an

160 important unique role in the signalling pathways used by the TCR and CD28 to control T cell
161 activation.
162
163 One prominent study has reported that *Pim1*/*Pim2* deficiency sensitises T cells to the
164 mTORc1 inhibitor rapamycin (Fox et al., 2005), which suggests mTORc1 can substitute for
165 the PIM kinases to control T cell activation. This previous study showed Pim dKO, but not
166 WT, naïve T cells cultured in IL-7 died in response to rapamycin treatment. It was also shown
167 that rapamycin synergised with *Pim1*/*Pim2*-deficiency to substantially reduce TCR-driven
168 activation and proliferation (Fox et al., 2005). However, we found no impact of *Pim1*/*Pim2*-
169 deficiency on the ability of naïve CD8 T cells cultured with IL-7 to survive in response to
170 rapamycin treatment (**Fig 1I**). Furthermore, we found no difference in the effect of
171 rapamycin on mean division number in αCD3/αCD28 activated Pim dKO versus WT CD8 T
172 cells (**Fig 1J**). Collectively these data show that PIM 1 and PIM2 are rapidly and strongly
173 expressed in response to immune activation, but they are dispensable for the antigen
174 receptor and CD28-driven proteome remodeling that initiates T cell clonal expansion and
175 differentiation. We also found no evidence that mTORc1 was substituting for *Pim1* and *Pim2*
176 loss.
177
178 ***PIM kinases do not control IL-15-driven CD8 T cell memory differentiation***
179 The proliferative expansion and differentiation programs of antigen activated CD8 T cells are
180 shaped by cytokines. In this context, PIM1 and PIM2 kinase expression is regulated by the
181 cytokines IL-2 and IL-15 which are key to shaping CD8 T cell effector and memory cell
182 differentiation respectively (Weninger et al., 2001; Cornish et al., 2006; Buck et al., 2016).
183 Both IL-2 and IL-15 upregulate PIM1 and PIM2 expression in antigen primed CD8 T cells (**Fig**
184 **2A**) and are required to sustain PIM1 and PIM2 expression (Rollings et al., 2018).
185 Accordingly, we assessed the contribution of PIM1 and PIM2 kinases to cytokine-driven
186 expansion and differentiation of antigen activated CD8 T cells. In these experiments,
187 antigen-primed CD8 T cells are expanded in IL-15 to generate memory phenotype CD8 T
188 cells or expanded in IL-2 to generate effector cytotoxic T lymphocytes (CTL) (Weninger et al.,
189 2001; Cornish et al., 2006; Buck et al., 2016) (**Fig 2B**).
190

191 Previous work has shown that PIM1 and PIM2 mediate IL-15 induced proliferation of gut
192 intra-epithelial lymphocytes (IEL) (James et al., 2021). However, their role in IL-15 responses
193 in conventional antigen receptor activated CD8 T cells is not known. We therefore first
194 examined the impact of *Pim1/Pim2*-deficiency on IL-15-driven conventional CD8 T cell
195 expansion. Antigen experienced WT CD8 T cells show a robust proliferative response to IL-
196 15 such that there is an ~90-fold expansion of the CD8 T cells between days 2 and 6 of
197 culture (**Fig 2C**). Immune activated Pim dKO CD8 T cells also proliferated strongly in
198 response to IL-15, but showed a moderate proliferative disadvantage resulting in a ~4-fold
199 difference in total cell number by day 6 of the culture (**Fig 2C**). There was no impact of
200 *Pim1*/*Pim2*-deficiency on the ability of IL-15 to sustain CD8 T cell viability (**Fig 2D**). Antigen-
201 primed CD8 T cells expand in IL-15 to generate memory phenotype CD8 T cells (Weninger et
202 al., 2001). We therefore examined whether *Pim1*/*Pim2*-deficiency had any impact on the
203 ability of IL-15 to induce memory differentiation. Accordingly, we performed parallel bulk
204 RNAseq and high-resolution mass spectrometry to analyse the transcriptome and proteome
205 of IL-15 expanded WT and Pim dKO CD8 T cells. The RNAseq analysis quantified ~14,000
206 unique polyA+ mRNA and using a cut off of >1.5 fold-change and q-value <0.05 we saw that
207 the abundance of 381 polyA+ RNA was modified by *Pim1*/*Pim2*-deficiency (**Fig 2E**) (**Table**
208 **S2A**). Of the 381 RNA that were detected as differentially expressed (FC>1.5, q<0.05) only
209 ~30% were detected with an average expression over 10 transcripts per million (TPM), of
210 these gene ~36% were non-coding RNA, uncharacterised genes or pseudogenes, leaving
211 only 72 substantially expressed protein coding mRNA that were differentially expressed in
212 Pim dKO versus WT IL-15 expanded CD8 T cells (**Table S2B**). These data indicate that
213 Pim1/Pim2-deficiency has very little effect on IL-15 induced protein-coding mRNA
214 expression in differentiated T cells. We then specifically examined if Pim dKO T cells had any
215 differences in mRNA that are known to be critical for memory cell differentiation. We found
216 that *Pim1*/*Pim2*-deficiency did not decrease expression of mRNA levels for critical memory T
217 cell genes such as the adhesion molecules and chemokine receptors, *Sell* (CD62L), *Ccr7* and
218 *S1pr1* that direct the trafficking of CD8 T cells to secondary lymphoid tissue. (**Fig 2F**).
219 *Pim1/Pim2*-deficiency also did not reduce expression of mRNA for the key memory cell
220 transcription factors *Tcf7, Foxo1, Foxo3 Klf2 and Id3.* (**Fig 2G**). Indeed, if anything, there
221 were small increases in expression of the *Klf2*, *Id3* and *Ccr7* mRNA in Pim dKO versus WT IL-
222 15 expanded CD8 T cells (**Fig 2F-G**).

223 Critically, when the proteomes of IL-15 expanded WT and Pim dKO CD8 T cells were
224 analysed and expression of ~6900 total proteins quantified, there were no major changes in
225 the proteomes between WT and Pim dKO IL-15 expanded CD8 T cells (**Fig 2H, Table S3**). Of
226 note, the mitochondrial proteome composition of IL-15 expanded WT and Pim dKO CD8 T
227 cells were indistinguishable (**Fig 2I-J**). This is pertinent because one key feature of how IL-15
228 controls memory T cells is via mitochondrial remodelling to support energy production via
229 oxidative phosphorylation and fatty acid oxidation (Buck et al., 2016) and it has been
230 described that PIM kinases can control mitochondrial phenotypes in cancer cell lines and
231 cardiomyocytes (Din et al., 2013; Chauhan et al., 2020). These data show that PIM1 and
232 PIM2 do not drive IL-15-mediated metabolic or differentiation programs in antigen-primed
233 CD8 T cells.
234
235 ***PIM kinases selectively modulate IL-2 controlled effector CD8 T cell differentiation***
236 IL-2 promotes the expression of PIM1 and PIM2 kinases (**Fig 2A**) and in this context, we
237 noted that the copy numbers per cell of PIM1 protein is considerably higher in actively
238 expanding antigen-activated CD8 cells maintained with IL-2 compared to IL-15 (**Fig 3A**)**.** We
239 therefore examined the role of PIM1 and PIM2 in the IL-2 signalling pathways that control
240 the differentiation of effector CTL. The data show that Pim dKO antigen activated CD8 T cells
241 responded normally to IL-2 to induce STAT5 Y694 phosphorylation (**Fig 3B**). They also
242 express normal levels of the IL-2-receptor alpha chain, CD25, (**Fig 3C**), which is sustained by
243 STAT5. Antigen activated WT CD8 T cells have a strong survival and proliferative response to
244 IL-2 producing an ~270-fold expansion between days 2 and 6 of culture in saturating IL-2
245 concentrations (**Fig 3D**). There was no impact of *Pim1*/*Pim2*-deficiency on the ability of IL-2
246 to maintain CD8 T cell viability (**Fig 3E**) and Pim dKO cells CD8 T cells cultured in IL-2
247 proliferated robustly. They did however exhibit a very mild proliferative disadvantage
248 resulting in a ~2-fold difference in total cell number by day 6 of the culture (**Fig 3D).** We
249 then examined whether *Pim1*/*Pim2*-deficiency had any impact on the differentiation of Pim
250 dKO CD8 T cells into effector CTL. Expression of activation markers CD44 and CD71 in IL-2-
251 expanded CTL were similar between WT and Pim dKO CD8 T cells on days 3 and 6 of co-
252 cultures (**Fig 3F**). However, one consistent difference between IL-2 maintained WT and Pim
253 dKO CD8 T cells is that WT CTL downregulated expression of CD62L (L-selectin, *Sell*),
254 whereas the Pim dKO CTL sustained higher CD62L expression (**Fig 3G**). We also noted that IL-

255 2 maintained Pim dKO CTL had reduced forward and side scatter properties i.e were smaller
256 and less granular than corresponding WT CTL (**Fig 3F).**
257
258 To explore the apparent size change between Pim dKO and WT IL-2 expanded CTL, we used
259 high resolution mass spectrometry to compare the proteomes of day 6 IL-2 cultured WT and
260 Pim dKO CTL. These analyses quantified expression of ~6,900 proteins and showed a small
261 decrease in the total protein mass of IL-2 maintained Pim dKO CD8 T cells compared to WT
262 cells (**Fig 4A, Table S4**). The data showed down-regulation of the expression of 513 proteins
263 (>1.5 fold-change, q<0.05) in Pim dKO CTL along with increased copy numbers of 33 proteins
264 (**Fig 4B**, **Table S4**). The transcription factor profile of Pim dKO T cells was consistent with
265 that of an effector CTL with high levels of TBX21 and low levels of TCF1 (*Tcf7*) (**Fig 4C**). Pim
266 dKO T cells also exhibited an effector-like mitochondrial proteome profile (**Fig S3**). However,
267 there were salient differences in proteins important for effector functionality between WT
268 and Pim dKO CD8 T cells. These included lower levels of the glucose transporters, SLC2A1
269 and SLC2A3 (GLUT1 and GLUT3) (**Fig 4D**) which are the major glucose transporters in CD8 T
270 cells (Hukelmann et al., 2016) and are key for enabling T cells to fuel high rates of glycolysis
271 and protein O-GlcNAcylation required to support effector functions (Chang et al., 2015;
272 Swamy et al., 2016). Pim dKO CTL also had decreased expression of a number of proteins
273 involved in fatty acid and cholesterol biosynthesis including SCD2, HMGCS1, MVK, IDI1,
274 FDPS, FDFT1 and SQLE (**Fig 4E**). Another striking observation was that the Pim dKO CD8 cells
275 had reduced levels of a number of key effector proteins including multiple granzymes,
276 perforin, IFNγ and TNFα (**Fig 4F-H**). Orthogonal flow cytometric analysis of Granzyme B and
277 IFNγ levels confirmed reduced levels of these effector molecule in IL-2 expanded Pim dKO
278 CTL, though IFNγ protein is only lowly produced in IL-2 maintained CTL (**Fig 4I).** In parallel
279 experiments we also examined the impact of an acute loss of PIM kinase activity on the
280 proteomes of IL-2 maintained CTL to see if this could recapitulate key observations from Pim
281 dKO T cells. When IL-2 maintained WT CTL were treated for 24 hours with the pan-PIM
282 kinases inhibitors PIM447 or AZD1208 we saw reductions in cell proliferation, cell size, cell
283 granularity, fatty acid biosynthesis proteins SCD1-3, glucose transporters SLC2A1, SLC2A3
284 and a reduction in Granzyme B expression (**Fig S4A-E, Table S5**). These experiments
285 corroborated some key observations from the experiments with Pim dKO CTL, where *Pim1*
286 and *Pim2* had been deleted over the lifespan of the T cell.

287

288 To examine the molecular regulation underpinning PIM1 and PIM2 kinase control of key
289 metabolic and effector proteins we also performed RNAseq on IL-2 differentiated WT and
290 Pim dKO CTL samples collected in parallel with the proteomics analysis described in Fig 4. In
291 these experiments ~14,000 polyA+ RNA were quantified and using a cut off >1.5 fold-
292 change, q<0.05 we saw that the abundance of 223 mRNA were decreased and 155 increased
293 by *Pim1*/*Pim2* deficiency (**Fig 5A, Table S6**). These data revealed that the reduced
294 expression of perforin and Granzymes C-G and K protein corresponded to decreases in their
295 mRNA (**Fig 5B-C**). However, there were striking examples where a clear decrease in protein
296 levels did not correspond with an appreciable decrease in mRNA expression. These included
297 the predominant cytolytic Granzymes B and A (**Fig 5C-D**), as well as both glucose
298 transporters SLC2A1 and SLC2A3 (**Fig 5E**). Furthermore, contrasting differential expression
299 of proteins and mRNA data in Pim dKO vs WT CTL revealed that ~75 % of the proteins whose
300 expression was changed in Pim dKO T cells (FC>1.5, q<0.05), exhibited no strong
301 corresponding changes in their mRNA (FC<1.2) (**Fig 5F, Table S7**). Indeed, of the ~500
302 proteins whose expression decreased at the protein level in Pim dKO CTL only 17 showed a
303 strong decrease in magnitude at the mRNA level as well (**Fig 5G, Table S7**).
304 These observations could reflect that the PIM kinases are required for IL-2 to maximally
305 control protein synthesis in CD8 T cells. To examine this hypothesis we first interrogated our
306 proteomics and transcriptomics data. Consistent with this hypothesis we observed a small
307 reduction in ribosome protein content in Pim dKO CTL, which scaled with the reduction in
308 total protein content (**Fig 5H**). Moreover, the translational repressor PDCD4 was increased
309 in Pim dKO CTL (**Fig 5I**). This could be confirmed by flow cytometry (**Fig 5J**) and was
310 underpinned at the mRNA level (**Fig 5B**). Similarly, 24 hour inhibition with pan PIM kinases
311 inhibitors was sufficient to substantially increase PDCD4 protein expression (**Fig S4F**). We
312 also noted that there was a small decrease in the expression of EIF4A1, a key component of
313 the eIF4F translation initiation complex, in Pim dKO IL-2 maintained CTL (**Fig 5K**). PDCD4
314 inhibits translation by binding EIF4A1 in a 2:1 ratio, preventing its interaction with the EIF4F
315 complex (Suzuki et al., 2008). Together the changes in both proteins equated to an
316 approximate halving of the ratio between EIF4A1 and PDCD4 (**Fig 5L**). These data all support
317 that loss of PIM kinases could reduce protein synthesis in IL-2 maintained CTL. To test this
318 hypothesis we used a single cell assay that quantifies the incorporation of an analogue of

319 puromycin (OPP) into newly synthesized protein chains in the ribosome to assess cellular
320 rates of protein synthesis. We found that 24 hours of treatment with pan-PIM kinase
321 inhibitors PIM447 or AZD1208 caused a quantitative reduction in protein synthesis rates of
322 IL-2 expanded CTL (**Fig 5M)**. This data is consistent with PIM kinase effects on protein
323 expression being via control of protein translation.
324
325 ***PIM1 and PIM2 regulate mTORc1 and sustain lymphoid homing in Pim1/Pim2-deficient***
326 ***effector CTL***
327 The pattern of proteome remodelling in Pim dKO CTL had some phenotypic features in
328 common with the previously reported changes that occur following inhibition of the
329 Serine/Threonine kinase mTORc1 in CTL (Hukelmann et al., 2016; Howden et al., 2019).
330 These included: increased expression of PDCD4 and decreased expression of cholesterol
331 biosynthesis enzymes and effector molecules including granzymes, perforin, IFNγ and TNFα
332 (Hukelmann et al., 2016; Howden et al., 2019). In this respect, mTORc1 activity in CTL is
333 acutely sensitive to reduced availability of glucose (Rolf et al., 2013) and the reduced
334 expression of glucose transporters in Pim dKO T cells might predict that these cells would
335 have lower activity of mTORc1. We therefore assessed if PIM kinases were required for IL-2
336 activation of mTORc1. In these experiments we compared the phosphorylation of S6K1 (p70
337 S6-kinase 1) on its mTORC1 substrate sequence T389 in WT and Pim dKO CD8 T cells by
338 western blot. These data show a modest reduction of mTORc1 activity in the Pim dKO T cells
339 (**Fig 6A**). We also assessed the activity of S6K1 at a single cell level by quantifying the
340 phosphorylation of its downstream target protein S6 ribosomal protein on S235/S236 by
341 flow cytometry over the course of IL-2 driven CTL expansion. These data also show that
342 *Pim1/Pim2*-deficiency reduced IL-2 induced mTORc1 dependent phosphorylation of S6 but
343 did not compromise the ability of the Pim dKO cells to phosphorylate S6 in response to
344 phorbol esters and calcium ionophores; pharmacological activators that induce RSK
345 mediated S6 phosphorylation (**Fig 6B**).
346
347 Previously, it has been shown that decreased glucose availability or inhibition of mTORc1
348 prevents the downregulation of CD62L that normally accompanies IL-2 induced CTL
349 differentiation (Sinclair et al., 2008; Finlay et al., 2012). Thus, the reduced expression of
350 glucose transporters and reduced activity of mTORc1 in Pim dKO IL-2 expanded CTL provides

351 a potential explanation for the striking phenotype shown in Fig 3G, that IL-2 maintained Pim
352 dKO CTL retain high levels of CD62L/L-selectin. The IL-2 CTL transcriptomics data showed
353 there is increased expression of CD62L at the mRNA level in IL-2 maintained PimdKO CTL (**Fig**
354 **5B, 6C**). The expression of *Sell* (CD62L) mRNA is controlled by the transcription factor KLF2
355 and the expression of *Klf2* mRNA is also increased in IL-2 maintained Pim dKO CTL (**Fig 6D**) as
356 are mRNA levels for other KLF2 targets: the chemokine receptors *Ccr7* and *S1pr1 (***Fig 6C***)*.
357
358 CD62L/L-selectin controls T cell adhesion to the endothelium of high endothelial venules
359 and is essential for lymphocyte transit from blood into secondary lymphoid tissue such as
360 lymph nodes. CCR7, and the $S1P_1$ receptor also direct migration by controlling T cell entry
361 and egress respectively into secondary lymphoid tissue. In this context, the loss of CD62L,
362 CCR7 and S1PR1 expression following immune activation reprograms the trafficking of
363 effector T cells away from lymphoid tissue toward sites of inflammation in peripheral tissues
364 (Sinclair et al., 2008; Nolz et al., 2011). Accordingly, the differences between Pim dKO and
365 WT CTL in terms of CD62L expression could indicate that in addition to having reduced
366 effector protein expression, Pim dKO CTL also do not switch their trafficking behaviour to
367 that of a fully differentiated effector CTL and rather retain the capacity to home to lymphoid
368 tissues. To test this possibility *in vivo*, we performed adoptive transfer experiments
369 comparing the ability of WT effector CTL and Pim dKO CTL to home to secondary lymphoid
370 tissues. In these experiments, αCD3/αCD28 activated WT or Pim dKO T cells were
371 differentiated in IL-2 and cells then were labelled with either CFSE or CTV dyes; mixed at a
372 ratio of 1:1, and adoptively transferred into C57BL/6 hosts. **Fig 6E** shows that Pim dKO CTL,
373 but not WT CTL, retained substantial capacity to home to secondary lymphoid organs and,
374 hence, accumulated in lymph nodes and spleen: PIM kinases are thus required for the
375 normal reprogramming of CTL trafficking.
376
377 **Discussion:**
378 The objective of the present study was to use quantitative analysis of T cell proteomes and
379 transcriptomes to explore how deletion of the Serine/Threonine kinases PIM1 and PIM2
380 impacts CD8 T cell activation and differentiation. The expression of PIM1 and PIM2 is
381 induced during immune activation of CD8 T cells by antigen and co-stimulation and then

382 sustained to varying degrees by the cytokines IL-2 or IL-15. The loss of PIM1 and PIM2 was
383 shown to have no effect on the CD8 T cell programs controlled by antigen receptor/co-
384 stimulation and had very little impact on the IL-15-driven transcriptional and proteomic
385 programs in memory differentiated CD8 T cells. However, PIM1 and PIM2 were required for
386 IL-2 programming of effector CD8 T cell differentiation. IL-2 controls essential cytolytic
387 effector and metabolic programs in CTL, is a key cytokine for CD8 T cell anti-viral immunity
388 and is also used to produce cytotoxic T cells for anti-cancer immunotherapy (Kalia and
389 Sarkar, 2018). The understanding that PIM kinases mediate IL-2 control of the expression of
390 glucose transporters, lipid metabolic enzymes and key cytolytic proteins such as granzymes
391 A and B in effector CD8 T cells is thus fundamental information about how this key cytokine
392 controls T cells. It was also important to understand that PIM kinases did not control the
393 transcriptional programs that direct expression of glucose transporters and effector
394 enzymes and the hence the full consequences of PIM kinase deletion could only be assessed
395 by in depth analysis of the proteomes of *Pim1*/*Pim2*-deficient CTL and not from mRNA
396 sequencing. The loss of PIM kinase activity reduced protein synthesis rates in CTL which
397 explains the discordance between mRNA and protein reported herein. The reduction in
398 protein synthesis was modest but previous studies have shown that modest reductions in
399 protein synthesis and loss of mTORc1 activity impact CD8 T cell differentiation programs
400 (Cornish et al., 2006; Hukelmann et al., 2016; Howden et al., 2019). PIM kinase regulation of
401 protein translation has been reported previously in mouse B cell lymphoma and mouse
402 embryonic fibroblasts (Schatz et al., 2011) and some of the key examples of proteins we
403 found to be unaltered at the mRNA level but down-regulated at the protein level have prior
404 reports of sensitivity to translational regulation in immune cells (Fehniger et al., 2007;
405 Ricciardi et al., 2018). Reduced protein synthesis capacity in cells lacking PIM kinases could
406 be caused by reduced mTORc1 activity combined with increased expression at the mRNA
407 and protein level of the translational repressor PDCD4. Moreover, protein synthesis is highly
408 energetically demanding and once CTL have reduced glucose transporter expression this
409 would reduce glucose availability to fuel protein production. These data collectively point
410 towards modulation of protein translation as an important target of PIM kinase activity
411 downstream of IL-2 in CD8 T cells.
412

413 One other important insight from the current work is that PIM kinases are required for IL-2
414 to fully repress expression of the adhesion molecule CD62L and the chemokine receptors
415 CCR7 and S1PR1. These molecules play a key role in controlling T cell homing to secondary
416 lymphoid tissue and are expressed at high levels in naïve and memory T cells. IL-2 induces
417 down regulation of CD62L, CCR7 and S1PR1 expression as part of a program that causes
418 effector cells to lose their capacity to home to secondary lymphoid tissues (Sinclair et al.,
419 2008; Nolz et al., 2011). The present data show that PIM kinases can mediate this IL-2
420 repression of lymph node homing receptors and the ability of IL-2 to switch off the naïve T
421 cell trafficking program. IL-2 maintained Pim dKO CD8 effector T cells thus retain the
422 capacity to home to secondary lymphoid tissues *in vivo*. This lymph-node homing pattern is
423 also a memory CD8 T cell phenotype but here it is pertinent that the current in-depth
424 analysis of the transcriptomes and proteomes of *Pim1*/*Pim2*-deficient IL-2 differentiated
425 CD8 T cells show that the loss of PIM kinases does not cause effector T cells to differentiate
426 instead into memory cells. For example, IL-2 maintained Pim dKO CD8 T cells do not re-
427 express key molecules that maintain the stem-like properties of memory cells such as the
428 transcription factor TCF7 and IL-7 receptor (Table S2, S6). Nor do Pim dKO CTL cultured in IL-
429 2 have the mitochondrial proteome of a memory T cell and PCA plots of IL-15 and IL-2
430 proteomics and RNAseq data show that Pim dKO IL-2 expanded CTL are still much more
431 similar to IL-2 expanded WT CTL than to IL-15 expanded CTL (Fig S5). Hence *Pim1*/*Pim2*-
432 deficiency prevents optimal differentiation of effector CTL but does not cause these cells to
433 fully switch to a memory phenotype. This is worth knowing as pan-PIM kinase inhibitors are
434 in development as anti-cancer drugs and it has been suggested that PIM inhibitors might be
435 used as a strategy to generate more stem-memory-like CD8 T cells in combination with
436 cancer immunotherapy treatments (Chatterjee et al., 2019; Clements and Warfel, 2022).
437 Information about how the loss of PIM kinases will impact CD8 T cells is very relevant to
438 informed usage of such drugs.
439
440 Finally, the selectivity of PIM kinases for IL-2 control of conventional CD8 T cell
441 differentiation with no evidence that PIMs were important for IL-15 responses beyond a
442 modest effect on cell proliferation was interesting. This failure to see a role for PIM
443 signalling in conventional peripheral CD8 T cell differentiation is in contrast to observations
444 that PIM1 and PIM2 direct IL-15 control of the metabolic programming of intestinal IEL

445 (James et al., 2021). A notable difference between these scenarios was that in IEL, IL-15 was
446 being used individually to drive immune activation and was sufficient to strongly induce
447 PIM1 and PIM2 expression. In contrast, in our conventional CD8 T cell system we uncovered
448 that IL-15 does not sustain high levels of PIM kinases, which could possibly explain this
449 discrepancy. However, high levels of PIM expression alone are not inevitably predictive of
450 their importance. In this study we observed very high levels of both PIM1 and PIM2 in
451 antigen activated CD8 T cells yet loss of PIM kinases there had no functional impact.
452 Previously it was suggested that mTORc1 could compensate for PIM kinase deficiency (Fox
453 et al., 2005). However we found no evidence for this, and in fact observed that PIM kinases
454 were required to maximally stimulate mTORc1 activity in IL-2 expanded CTL. Thus, this
455 examination of the role of PIM kinases in multiple signalling situations reveal cell context
456 dependent regulatory roles for PIM kinases rather than hard wired functions that apply to
457 every stimulatory situation in T cells.
458

459 **References:**

460 Aho, T. L., R. J. Lund, E. K. Ylikoski, S. Matikainen, R. Lahesmaa, and P. J. Koskinen. 2005.
461 Expression of human pim family genes is selectively up-regulated by cytokines
462 promoting T helper type 1, but not T helper type 2, cell differentiation. *Immunology*
463 116: 82-88.
464 Blagih, J., F. Coulombe, E. E. Vincent, F. Dupuy, G. Galicia-Vazquez, E. Yurchenko, T. C. Raissi,
465 et al. 2015. The energy sensor AMPK regulates T cell metabolic adaptation and
466 effector responses in vivo. *Immunity* 42: 41-54.
467 Brenes, A. J., A. I. Lamond, and D. A. Cantrell. 2023. The Immunological Proteome Resource.
468 *Nat Immunol* 24: 731.
469 Buchacher, T., A. Shetty, S. A. Koskela, J. Smolander, R. Kaukonen, A. G. G. Sousa, S. Junttila,
470 et al. 2023. PIM kinases regulate early human Th17 cell differentiation. *Cell Rep* 42:
471 113469.
472 Buck, M. D., D. O'Sullivan, R. I. Klein Geltink, J. D. Curtis, C. H. Chang, D. E. Sanin, J. Qiu, et al.
473 2016. Mitochondrial Dynamics Controls T Cell Fate through Metabolic Programming.
474 *Cell* 166: 63-76.
475 Bullock, A. N., J. Debreczeni, A. L. Amos, S. Knapp, and B. E. Turk. 2005. Structure and
476 substrate specificity of the Pim-1 kinase. *J Biol Chem* 280: 41675-41682.
477 Cantrell, D. 2015. Signaling in lymphocyte activation. *Cold Spring Harb Perspect Biol* 7.
478 Chang, C. H., J. Qiu, D. O'Sullivan, M. D. Buck, T. Noguchi, J. D. Curtis, Q. Chen, et al. 2015.
479 Metabolic Competition in the Tumor Microenvironment Is a Driver of Cancer
480 Progression. *Cell* 162: 1229-1241.
481 Chatterjee, S., P. Chakraborty, A. Daenthanasanmak, S. Iamsawat, G. Andrejeva, L. A.
482 Luevano, M. Wolf, et al. 2019. Targeting PIM Kinase with PD1 Inhibition Improves
483 Immunotherapeutic Antitumor T-cell Response. *Clin Cancer Res* 25: 1036-1049.
484 Chauhan, S. S., R. K. Toth, C. C. Jensen, A. L. Casillas, D. F. Kashatus, and N. A. Warfel. 2020.
485 PIM kinases alter mitochondrial dynamics and chemosensitivity in lung cancer.
486 *Oncogene* 39: 2597-2611.
487 Clements, A. N., and N. A. Warfel. 2022. Targeting PIM Kinases to Improve the Efficacy of
488 Immunotherapy. *Cells* 11.
489 Cornish, G. H., L. V. Sinclair, and D. A. Cantrell. 2006. Differential regulation of T-cell growth
490 by IL-2 and IL-15. *Blood* 108: 600-608.
491 Damasio, M. P., J. M. Marchingo, L. Spinelli, J. L. Hukelmann, D. A. Cantrell, and A. J. M.
492 Howden. 2021. Extracellular signal-regulated kinase (ERK) pathway control of CD8+ T
493 cell differentiation. *Biochem J* 478: 79-98.
494 Din, S., M. Mason, M. Volkers, B. Johnson, C. T. Cottage, Z. Wang, A. Y. Joyo, et al. 2013. Pim-
495 1 preserves mitochondrial morphology by inhibiting dynamin-related protein 1
496 translocation. *Proc Natl Acad Sci U S A* 110: 5969-5974.
497 Dobin, A., C. A. Davis, F. Schlesinger, J. Drenkow, C. Zaleski, S. Jha, P. Batut, et al. 2013. STAR:
498 ultrafast universal RNA-seq aligner. *Bioinformatics* 29: 15-21.
499 Ewels, P., M. Magnusson, S. Lundin, and M. Kaller. 2016. MultiQC: summarize analysis results
500 for multiple tools and samples in a single report. *Bioinformatics* 32: 3047-3048.
501 Fehniger, T. A., S. F. Cai, X. Cao, A. J. Bredemeyer, R. M. Presti, A. R. French, and T. J. Ley.
502 2007. Acquisition of murine NK cell cytotoxicity requires the translation of a pre-
503 existing pool of granzyme B and perforin mRNAs. *Immunity* 26: 798-811.

504 Finlay, D. K., E. Rosenzweig, L. V. Sinclair, C. Feijoo-Carnero, J. L. Hukelmann, J. Rolf, A. A.
505 Panteleyev, et al. 2012. PDK1 regulation of mTOR and hypoxia-inducible factor 1
506 integrate metabolism and migration of CD8+ T cells. *J Exp Med* 209: 2441-2453.
507 Fox, C. J., P. S. Hammerman, and C. B. Thompson. 2005. The Pim kinases control rapamycin-
508 resistant T cell survival and activation. *J Exp Med* 201: 259-266.
509 Fox, C. J., P. S. Hammerman, R. M. Cinalli, S. R. Master, L. A. Chodosh, and C. B. Thompson.
510 2003. The serine/threonine kinase Pim-2 is a transcriptionally regulated apoptotic
511 inhibitor. *Genes Dev* 17: 1841-1854.
512 Howden, A. J. M., J. L. Hukelmann, A. Brenes, L. Spinelli, L. V. Sinclair, A. I. Lamond, and D. A.
513 Cantrell. 2019. Quantitative analysis of T cell proteomes and environmental sensors
514 during T cell differentiation. *Nat Immunol* 20: 1542-1554.
515 Hughes, C. S., S. Foehr, D. A. Garfield, E. E. Furlong, L. M. Steinmetz, and J. Krijgsveld. 2014.
516 Ultrasensitive proteome analysis using paramagnetic bead technology. *Mol Syst Biol*
517 10: 757.
518 Hukelmann, J. L., K. E. Anderson, L. V. Sinclair, K. M. Grzes, A. B. Murillo, P. T. Hawkins, L. R.
519 Stephens, et al. 2016. The cytotoxic T cell proteome and its shaping by the kinase
520 mTOR. *Nat Immunol* 17: 104-112.
521 Jackson, L. J., J. A. Pheneger, T. J. Pheneger, G. Davis, A. D. Wright, J. E. Robinson, S. Allen, et
522 al. 2012. The role of PIM kinases in human and mouse CD4+ T cell activation and
523 inflammatory bowel disease. *Cell Immunol* 272: 200-213.
524 James, O. J., M. Vandereyken, J. M. Marchingo, F. Singh, S. E. Bray, J. Wilson, A. G. Love, and
525 M. Swamy. 2021. IL-15 and PIM kinases direct the metabolic programming of
526 intestinal intraepithelial lymphocytes. *Nat Commun* 12: 4290.
527 Kalia, V., and S. Sarkar. 2018. Regulation of Effector and Memory CD8 T Cell Differentiation by
528 IL-2-A Balancing Act. *Front Immunol* 9: 2987.
529 Knudson, K. M., C. J. Pritzl, V. Saxena, A. Altman, M. A. Daniels, and E. Teixeiro. 2017.
530 NFkappaB-Pim-1-Eomesodermin axis is critical for maintaining CD8 T-cell memory
531 quality. *Proc Natl Acad Sci U S A* 114: E1659-E1667.
532 Laird, P. W., N. M. van der Lugt, A. Clarke, J. Domen, K. Linders, J. McWhir, A. Berns, and M.
533 Hooper. 1993. In vivo analysis of Pim-1 deficiency. *Nucleic Acids Res* 21: 4750-4755.
534 Law, C. W., M. Alhamdoosh, S. Su, X. Dong, L. Tian, G. K. Smyth, and M. E. Ritchie. 2016. RNA-
535 seq analysis is easy as 1-2-3 with limma, Glimma and edgeR. *F1000Res* 5.
536 Lawrence, M., W. Huber, H. Pages, P. Aboyoun, M. Carlson, R. Gentleman, M. T. Morgan, and
537 V. J. Carey. 2013. Software for computing and annotating genomic ranges. *PLoS*
538 *Comput Biol* 9: e1003118.
539 Li, H., L. Xie, L. Zhu, Z. Li, R. Wang, X. Liu, Z. Huang, et al. 2022. Multicellular immune
540 dynamics implicate PIM1 as a potential therapeutic target for uveitis. *Nat Commun*
541 13: 5866.
542 Locard-Paulet, M., G. Voisinne, C. Froment, M. Goncalves Menoita, Y. Ounoughene, L. Girard,
543 C. Gregoire, et al. 2020. LymphoAtlas: a dynamic and integrated phosphoproteomic
544 resource of TCR signaling in primary T cells reveals ITSN2 as a regulator of effector
545 functions. *Mol Syst Biol* 16: e9524.
546 Maney, N. J., H. Lemos, B. Barron-Millar, C. Carey, I. Herron, A. E. Anderson, A. L. Mellor, et
547 al. 2021. Pim Kinases as Therapeutic Targets in Early Rheumatoid Arthritis. *Arthritis*
548 *Rheumatol* 73: 1820-1830.

549 Marchingo, J. M., L. V. Sinclair, A. J. Howden, and D. A. Cantrell. 2020. Quantitative analysis of
550 how Myc controls T cell proteomes and metabolic pathways during T cell activation.
551 *Elife* 9.
552 Matikainen, S., T. Sareneva, T. Ronni, A. Lehtonen, P. J. Koskinen, and I. Julkunen. 1999.
553 Interferon-alpha activates multiple STAT proteins and upregulates proliferation-
554 associated IL-2Ralpha, c-myc, and pim-1 genes in human T cells. *Blood* 93: 1980-
555 1991.
556 McCarthy, D. J., Y. Chen, and G. K. Smyth. 2012. Differential expression analysis of multifactor
557 RNA-Seq experiments with respect to biological variation. *Nucleic Acids Res* 40: 4288-
558 4297.
559 McCarthy, D. J., K. R. Campbell, A. T. Lun, and Q. F. Wills. 2017. Scater: pre-processing, quality
560 control, normalization and visualization of single-cell RNA-seq data in R.
561 *Bioinformatics* 33: 1179-1186.
562 Mikkers, H., M. Nawijn, J. Allen, C. Brouwers, E. Verhoeven, J. Jonkers, and A. Berns. 2004.
563 Mice deficient for all PIM kinases display reduced body size and impaired responses
564 to hematopoietic growth factors. *Mol Cell Biol* 24: 6104-6115.
565 Navarro, M. N., J. Goebel, J. L. Hukelmann, and D. A. Cantrell. 2014. Quantitative
566 phosphoproteomics of cytotoxic T cells to reveal protein kinase d 2 regulated
567 networks. *Mol Cell Proteomics* 13: 3544-3557.
568 Navarro, M. N., J. Goebel, C. Feijoo-Carnero, N. Morrice, and D. A. Cantrell. 2011.
569 Phosphoproteomic analysis reveals an intrinsic pathway for the regulation of histone
570 deacetylase 7 that controls the function of cytotoxic T lymphocytes. *Nat Immunol* 12:
571 352-361.
572 Nolz, J. C., G. R. Starbeck-Miller, and J. T. Harty. 2011. Naive, effector and memory CD8 T-cell
573 trafficking: parallels and distinctions. *Immunotherapy* 3: 1223-1233.
574 Peng, C., A. Knebel, N. A. Morrice, X. Li, K. Barringer, J. Li, S. Jakes, et al. 2007. Pim kinase
575 substrate identification and specificity. *J Biochem* 141: 353-362.
576 Peperzak, V., E. A. Veraar, A. M. Keller, Y. Xiao, and J. Borst. 2010. The Pim kinase pathway
577 contributes to survival signaling in primed CD8+ T cells upon CD27 costimulation. *J*
578 *Immunol* 185: 6670-6678.
579 Ricciardi, S., N. Manfrini, R. Alfieri, P. Calamita, M. C. Crosti, S. Gallo, R. Muller, et al. 2018.
580 The Translational Machinery of Human CD4(+) T Cells Is Poised for Activation and
581 Controls the Switch from Quiescence to Metabolic Remodeling. *Cell Metab* 28: 961.
582 Ritchie, M. E., B. Phipson, D. Wu, Y. Hu, C. W. Law, W. Shi, and G. K. Smyth. 2015. limma
583 powers differential expression analyses for RNA-sequencing and microarray studies.
584 *Nucleic Acids Res* 43: e47.
585 Robinson, M. D., D. J. McCarthy, and G. K. Smyth. 2010. edgeR: a Bioconductor package for
586 differential expression analysis of digital gene expression data. *Bioinformatics* 26:
587 139-140.
588 Rolf, J., M. Zarrouk, D. K. Finlay, M. Foretz, B. Viollet, and D. A. Cantrell. 2013. AMPKalpha1: a
589 glucose sensor that controls CD8 T-cell memory. *Eur J Immunol* 43: 889-896.
590 Rollings, C. M., L. V. Sinclair, H. J. M. Brady, D. A. Cantrell, and S. H. Ross. 2018. Interleukin-2
591 shapes the cytotoxic T cell proteome and immune environment-sensing programs.
592 *Sci Signal* 11.
593 Saravia, J., J. L. Raynor, N. M. Chapman, S. A. Lim, and H. Chi. 2020. Signaling networks in
594 immunometabolism. *Cell Res* 30: 328-342.

595 Schatz, J. H., E. Oricchio, A. L. Wolfe, M. Jiang, I. Linkov, J. Maragulia, W. Shi, et al. 2011.
596 Targeting cap-dependent translation blocks converging survival signals by AKT and
597 PIM kinases in lymphoma. *J Exp Med* 208: 1799-1807.
598 Sinclair, L. V., D. Finlay, C. Feijoo, G. H. Cornish, A. Gray, A. Ager, K. Okkenhaug, et al. 2008.
599 Phosphatidylinositol-3-OH kinase and nutrient-sensing mTOR pathways control T
600 lymphocyte trafficking. *Nat Immunol* 9: 513-521.
601 Sinclair, L. V., A. J. Howden, A. Brenes, L. Spinelli, J. L. Hukelmann, A. N. Macintyre, X. Liu, et
602 al. 2019. Antigen receptor control of methionine metabolism in T cells. *Elife* 8.
603 Sollberger, G., A. J. Brenes, J. Warner, J. S. C. Arthur, and A. J. M. Howden. 2023. Quantitative
604 proteomics reveals tissue-specific, infection-induced and species-specific neutrophil
605 protein signatures. *bioRxiv* 10.1101/2023.09.05.556395 DOI:
606 2023.2009.2005.556395.
607 Spinelli, L., J. M. Marchingo, A. Nomura, M. P. Damasio, and D. A. Cantrell. 2021.
608 Phosphoinositide 3-Kinase p110 Delta Differentially Restrains and Directs Naive
609 Versus Effector CD8(+) T Cell Transcriptional Programs. *Front Immunol* 12: 691997.
610 Storey, J. D., A. J. Bass, A. Dabney, and D. Robinson. 2023. qvalue: Q-value estimation for
611 false discovery rate control, version R package version 2.32.0.
612 Suzuki, C., R. G. Garces, K. A. Edmonds, S. Hiller, S. G. Hyberts, A. Marintchev, and G. Wagner.
613 2008. PDCD4 inhibits translation initiation by binding to eIF4A using both its MA3
614 domains. *Proc Natl Acad Sci U S A* 105: 3274-3279.
615 Swamy, M., S. Pathak, K. M. Grzes, S. Damerow, L. V. Sinclair, D. M. van Aalten, and D. A.
616 Cantrell. 2016. Glucose and glutamine fuel protein O-GlcNAcylation to control T cell
617 self-renewal and malignancy. *Nat Immunol* 17: 712-720.
618 Tan, H., K. Yang, Y. Li, T. I. Shaw, Y. Wang, D. B. Blanco, X. Wang, et al. 2017. Integrative
619 Proteomics and Phosphoproteomics Profiling Reveals Dynamic Signaling Networks
620 and Bioenergetics Pathways Underlying T Cell Activation. *Immunity* 46: 488-503.
621 Warfel, N. A., and A. S. Kraft. 2015. PIM kinase (and Akt) biology and signaling in tumors.
622 *Pharmacol Ther* 151: 41-49.
623 Weninger, W., M. A. Crowley, N. Manjunath, and U. H. von Andrian. 2001. Migratory
624 properties of naive, effector, and memory CD8(+) T cells. *J Exp Med* 194: 953-966.
625 Wingett, D., A. Long, D. Kelleher, and N. S. Magnuson. 1996. pim-1 proto-oncogene
626 expression in anti-CD3-mediated T cell activation is associated with protein kinase C
627 activation and is independent of Raf-1. *J Immunol* 156: 549-557.
628 Wisniewski, J. R., M. Y. Hein, J. Cox, and M. Mann. 2014. A "proteomic ruler" for protein copy
629 number and concentration estimation without spike-in standards. *Mol Cell*
630 *Proteomics* 13: 3497-3506.
631 Xin, G., Y. Chen, P. Topchyan, M. Y. Kasmani, R. Burns, P. J. Volberding, X. Wu, et al. 2021.
632 Targeting PIM1-Mediated Metabolism in Myeloid Suppressor Cells to Treat Cancer.
633 *Cancer Immunol Res* 9: 454-469.
634 Zougman, A., P. J. Selby, and R. E. Banks. 2014. Suspension trapping (STrap) sample
635 preparation method for bottom-up proteomics analysis. *Proteomics* 14: 1006-1000.
636

637

638

639

640 **Acknowledgements:**
641 The authors thank members of the Cantrell group for their critical discussion of the data, in
642 particular we thank Linda Sinclair for critical reading and comments on the manuscript. We
643 thank Victor Tybulewicz for providing the Pim1-/- and Pim2-/- mice, E Emslie for help with
644 mouse maintenance and experimental support, B Stubbs for technical assistance with
645 mouse genotyping, A Brenes for assistance with analytical tools, A Gardner, A Rennie and R
646 Clarke from the Flow Cytometry facility for cell sorting, K Beattie and A Atrih from the
647 Fingerprint proteomics facility for performed mass spectrometry, S Thomson for assistance
648 with adoptive transfer experiments, the Biological Resource Unit at the University of
649 Dundee and the Finnish Functional Genomics Centre, University of Turku and Abo Akademi
650 Biocenter Finland for performing RNA sequencing. This research was supported by a
651 Wellcome Trust Principal Research Fellowship to DAC (205023/Z/16/Z), a Wellcome Trust
652 Equipment Award to DAC (202950/Z/16/Z), an EMBO Long term Fellowship (ALTF 1543–
653 2015) and NHMRC CJ Martin Early Career fellowship (APP1120748) to JMM and has received
654 funding from the European Union's Horizon 2020 research and innovation programme
655 under the Marie Skłodowska-Curie grant agreement No 705984 to JMM and DAC.

656 **Materials and Methods:**

657 **Mice**

658 Pim1$^{-/-}$ (Pim1 KO)(Laird et al., 1993) and Pim2$^{-/-}$ or Pim2$^{-/Y}$ (Pim2 KO) mice (Mikkers et al.,
659 2004) on the FVB/N background were backcrossed for >10 generations onto a C57BL/6
660 background and were a generous gift from Prof Victor Tybulewicz. Pim1 KO and Pim2 KO
661 mice were inter-crossed to generate the Pim1/Pim2 double KO (Pim dKO) strain. Pim dKO,
662 C57BL/6, Ly5.1, P14 and OT1 mice were bred and maintained in the WTB/RUTG, University
663 of Dundee in compliance with UK Home Office Animals (Scientific Procedures) Act 1986
664 guidelines. Mice used for proteomics and RNAseq studies were male and 12-15 weeks of
665 age. Age/sex matched mice were used for all other experiments between 5–52 weeks of
666 age, with most being between 10 – 20 weeks.

667

668 **Cell culture**

669 Single cell suspensions were generated by mashing mouse lymph nodes (brachial, axial,
670 inguinal, superficial cervical, deep cervical, lumbar) or spleens through a 70 µm strainer. Red
671 blood cells were lysed with Ack buffer (150 mM NH_4Cl 10 mM $KHCO_3$110 µM Na_2EDTA pH
672 7.8). Cells were cultured in RPMI 1640 containing glutamine (Invitrogen), supplemented
673 with 10% FBS (Gibco), penicillin/streptomycin (Gibco) and 50 µM β-mercaptoethanol
674 (Sigma) at 37 °C with 5% CO_2.

675

676 For 24 hour TCR activation WT and Pim dKO proteomics and phenotyping, lymph node
677 suspension from 2 mice per biological replicate were activated with 0.5 µg/mL anti-mouse
678 CD3 (Biolegend) and 0.5 µg/mL anti-mouse CD28 (eBioscience) in 2 × 10 mL complete
679 culture medium in six well plates. Proteomics samples were generated in biological
680 triplicate.

681

682 For generation of memory-like or effector cytotoxic T lymphocytes (CTL) from mice with
683 polyclonal T cell repertoires, LN or spleen single cell suspensions at an equal density for WT
684 and Pim dKO cultures (~1-3 million live cells/mL) were activated with 0.5 µg/mL anti-mouse
685 CD3 (Biolegend) and 0.5 µg/mL anti-mouse CD28 (eBioscience) and recombinant human IL-
686 15 (20 ng/mL, Peprotech) or recombinant human IL-2 (20 ng/mL, Proleukin, Novartis) in 10
687 mL complete culture medium. After 2 days of activation (~40 hours) cells were washed out

688 of activation medium and resuspended at 0.3 million T cells/mL in fresh culture medium and
689 cytokine 20 ng/mL of IL-15 or IL-2 for memory-like and effector T cells respectively. T cells
690 were subsequently split into fresh medium and cytokine daily at a density of 0.5 million/ mL
691 and 0.3 million/mL for memory-like and effector T cells respectively until analysis timepoint.
692
693 For generation of effector CTL from TCR-transgenic P14 mice LN single cell suspensions were
694 activated with 100 ng/mL gp33 peptide, recombinant human IL-2 (20 ng/mL) and
695 recombinant mouse IL12 (2 ng/mL) (Peprotech) for 2 days, before washing out of activation
696 media and splitting cells daily into fresh media containing IL-2 (20 ng/mL) at a density of 0.3
697 million/mL.
698
699 For co-culture experiments Ly5.1+ WT and Pim dKO (Ly5.2+) cell suspensions were mixed in
700 a 50:50 ratio based on total T cell numbers before activation. A portion of the mixed naïve T
701 cells maintained in recombinant mouse IL-7 (5 ng/mL, Peprotech) to verify baseline T cell
702 ratios over time in culture.
703
704 For experiments where a pure CD8+ CTL population were required from non-TCR transgenic
705 mice (adoptive transfer, proteomics and RNAseq experiments), CD4 T cells were depleted
706 on day 3 of CTL cultures (i.e. 24 hours after being washed out of initial activation conditions)
707 by negative magnetic selection. T cells were resuspended in MACS buffer (PBS, 1mM EDTA,
708 2%FBS) at 10^8/mL, blocked with 50 µL/mL Rat Serum, incubated for 10 min with anti-CD4
709 biotin antibody (5 µg/mL, Biolegend), incubated for 5 min with 125 µL/mL RapidSphere
710 beads (StemCell Technologies), then volume topped up to 2.5 mL and placed in EasySep
711 magnet for 2.5 min. Supernatant containing CD8 T cells was collected and returned to
712 culture as per CTL protocol above. CD4 T cell depletion was confirmed by flow cytometry,
713 with CD4+ cells making up <0.4% of live cells.
714
715 In experiments where cytokine was withdrawn T cells were washed at least twice with warm
716 complete medium. Where indicated CTL were treated with 100 nM Tofacitinib
717 (Selleckchem), 20 nM of rapamycin (Merck), 20 ng/mL PDBu (Cell Signaling Technologies)
718 and ionomycin 500 ng/mL (Merck) or the pan PIM kinase inhibitors PIM447 (1 or 5 µM as
719 indicated) and AZD1208 (1 or 10 µM as indicated) (both Medchemexpress).

720 **Flow cytometry**

721 Flow cytometry data was acquired on a FACSVerse using FACSuite software, FACSCanto, or
722 LSR II Fortessa with FACS DIVA software (BD Biosciences) or Novocyte (Acea Biosciences
723 Inc.) with NovoExpress software (Agilent). Data was analysed using Flowjo software version
724 9.9.6 or version 10.6.1 and above (Treestar).

725 Cell surface staining antibodies conjugated to BV421, BV510, V500, FITC, PE, PerCPCy5.5,
726 PECy7, APC, A647 and APCeF780 were obtained from BD Biosciences, eBioscience or
727 Biolegend. Fc receptors were blocked using Fc block (BD Biosciences). Antibody staining for
728 surface markers was performed at 1:200 in PBS 1%FBS. Antibody clones were as follows:
729 CD4 (RM4-5), CD8 (53–6.7), CD25 (7D4 or PC61), CD44 (IM7), CD45.1 (A20), CD45.2 (104),
730 CD62L (MEL-14), CD69 (H1.2F), CD71 (RI7217), TCRbeta (H57-597).

731

732 For IFNγ and Granzyme B intracellular staining cells were fixed and permeabilised using
733 eBioscience Intracellular Fixation and Permeabilisation kit (eBioscience) as per manufacturer
734 instructions. Cells were stained with anti-IFNγ (XMG1.2) and anti-Granzyme B (NGZB) at
735 1:100 and 1:200 respectively. For intracellular IFNγ staining GolgiPlug (BD) was added to the
736 culture 4 hours prior to analysis.

737 For intracellular phospho S6 staining cells were fixed with 0.5% paraformaldehyde at 37 ^{o}C
738 and permeabilised with ice cold 90% methanol. Cells were stained at 1:100 with anti-
739 phospho S6 ribosomal protein (Ser235/236) Alexa Fluor 647 (D57.2.2E, Cell Signaling
740 Technologies cat#4851S).

741 For intracellular phospho-STAT5 staining cells were fixed with 1% paraformaldehyde at
742 room temperature and permeabilised with ice cold 90% methanol. Cells were stained at
743 1:200 with rabbit anti-phospho STAT5 (Y694) (C11C5, Cell Signaling Technologies cat#9359S)
744 followed by anti-rabbit IgG Fab2 Alexa Fluor 647 (Cell Signaling Technologies cat#4414S).

745 For intracellular PDCD4 staining cells were fixed with 1% paraformaldehyde at room
746 temperature and permeabilised with Perm Buffer (eBioscience, cat# 00-8333-56). Cells were
747 stained at 1:100 with rabbit anti-PDCD4 (D29C6, Cell Signaling Technologies cat#9535S)
748 followed by anti-rabbit IgG Fab2 Alexa Fluor 647 (Cell Signaling Technologies cat#4414S).

749

750

751

752 **Cell sorting**

753 Cell sorting was performed on a Sony SH800S cell sorter (Sony Biotechnology). Staining was
754 performed in PBS 1% FBS and sorting and collection of cells for proteomics analysis was
755 performed in RPMI 1640 containing glutamine, supplemented with 1% FBS. 24 hour TCR
756 activated WT and Pim dKO CD4 and CD8 T cells were sorted as: DAPI-CD69+ CD8+ or CD4+.
757 Cells were washed twice with HBSS (no calcium, no magnesium, no phenol red, GIBCO)
758 before being snap frozen in liquid nitrogen and stored at −80°C until further processing.
759

760 **CTL number estimation and viability**

761 Absolute CD8 T cell number per well/flask and % live cells was assessed in CTL cultures by
762 volumetric measurement of cell number from 50 µL culture medium. Cells were transferred
763 into 450 µL PBS containing low concentration anti-CD8, anti-CD4 antibody (both 1:1500) and
764 DAPI (1 µg/mL, Thermofisher Scientific) or propidium iodide (0.2 µg/mL, Sigma) and cell
765 number and viability assessed on either FACSVerse or Novocyte flow cytometers. Estimated
766 live cell counts were corrected for assay dilution ratio, total culture volume and splitting
767 ratios for each time point. Proportions of CD8 T cells that were Ly5.1+ or Ly5.2+ from
768 parallel surface staining were used to calculate WT and Pim dKO numbers respectively in co-
769 culture experiments.
770

771 **CTV proliferation assay**

772 For CTV proliferation assay, lymph node suspensions at 10^7 cells per mL in PBS 0.5%FCS
773 were labelled with 5 µM CTV (Invitrogen) for 20 min at 37°C before reaction was quenched
774 and cells washed with cold medium. 10^5 live cells were activated with αCD3/αCD28 (both
775 0.5 µg/mL) or maintained in IL-7 (5 ng/mL) +/- rapamycin (20 nM) in 200 µL total volume in
776 96 well flat-bottomed plates. Propidium iodide (0.2 µg/mL), low dose αCD4, αCD8 antibody
777 (both 1:3200 final concentration) and 10,000 sphero rainbow beads (BD) were added to
778 wells prior to analysis of beads number, cell number, cell viability, CD4 and CD8 T cell
779 composition and CTV profile of samples by flow cytometry. The ratio between the known
780 number of beads added to the number of beads measured per well was multiplied with the
781 number of cells measured to calculate the absolute cell number per well. Cell number per
782 division was then corrected for the effect of expansion by dividing cell number per division

783 by 2^division number and the arithmetic mean division number calculated from these
784 values.
785
786 **Protein synthesis assay**
787 To assess protein synthesis cells were cultured with 20 µM O-propargyl puromycin (OPP,
788 Jena Bioscience) for 10 min. Control cells were cultured with cycloheximide (100 µg/mL,
789 Sigma-Aldrich) for 20 min prior to addition of OPP to assess background staining level when
790 cytosolic protein synthesis is completely inhibited. Cells were washed, fixed with 1% PFA,
791 permeabilised with 0.5% Triton x-100 and OPP incorporation into newly synthesised
792 peptides was measured by conjugating with Alexa647-azide via a Click-IT chemistry reaction
793 (2 µM Alexa-647-azide, 2 mM $CuSO_4$, 5 mM ascorbic acid in PBS) (Invitrogen) and assessing
794 fluorescence by flow cytometry.
795
796 **Adoptive Transfer**
797 WT and Pim dKO CD8 T cells were activated and expanded in IL-2 as described above. On
798 day 6 of culture WT and Pim dKO CTL were labelled with either CTV, or 5 µM CFSE
799 (Invitrogen) as per CTV assay protocol described above, with the exception that labelling
800 was performed in RPMI 1640 and CFSE labelling was for 10 min. CTV and CFSE labelling was
801 alternated between genotypes across biological replicates to prevent any potential
802 introduction of bias due to possible differences in dye toxicity. Labelled WT and Pim dKO
803 CD8 T cells were mixed in a 50:50 ratio and 5 million cells/mouse were adoptively
804 transferred via intravenous tail injection into C57BL/6 recipient mice. Recipient mice were
805 sacrificed and blood, spleen and lymph nodes (axillary, brachial and inguinal) removed 4 and
806 23 hours post-transfer and the ratio of CTV to CFSE cells assessed by flow cytometry.
807
808 **Western blotting**
809 Cell pellets were lysed in RIPA buffer (100 mM HEPES, pH 7.4, 150 mM NaCl, 1% NP40, 0.1%
810 SDS, 0.5% sodium deoxycholate, 10% glycerol, 1 mM EDTA, 1 mM EGTA, 1 mM TCEP, and
811 protease and phosphatase inhibitors (Roche)) at 20 million T cells/mL at 4 ^{o}C. Lysates were
812 sonicated, centrifuged 12 min, 13,000 rpm, 4°C. Supernatant was transferred to fresh tube
813 and NuPAGE LDS sample buffer (1×) (Life Technologies) and tris(2-carboxyethyl)phosphine
814 (TCEP, 25mM, Thermofisher) was added before boiling samples at 100°C for 3 min. Samples

815 were loaded and separated by SDS-PAGE (NuPAGE 4-12% gradient precast gels
816 (ThermoFisher) or 12% polyacrylamide running gel), and then transferred to nitrocellulose
817 membranes (Whatman). Equal cell numbers (~140,000 cells) were loaded per lane. Blots
818 were probed with the following primary antibodies: S6K (5G10, Cell Signaling Technology,
819 cat# 2217S), S6K p-T389 (108D2, Cell Signaling Technology, cat# 9234S), STAT5 p-Y694
820 (C11C5, Cell Signalling Technology, cat# 9359S), Pim1 (12H8, Santa Cruz, cat# SC-13513),
821 Pim2 (1D12, Santa Cruz, cat# SC-13514). Horseradish peroxidase (HRP)-conjugated anti-
822 rabbit or anti-mouse secondary antibodies were used to assess protein signal (Thermo
823 Scientific, Cell Signaling Technologies). Chemiluminescence was measured using an Odyssey
824 Fc Imaging System (Licor) and Image Studio Software (LI-COR) was used to quantify
825 chemiluminescence.
826
827 **Proteomics:**
828 **Proteomics sample preparation**
829 Cell pellets for 24 hour TCR WT and Pim dKO CD4 and CD8 T cells were activated and sorted
830 as described above.
831
832 IL-2 and IL-15 expanded WT and Pim dKO CD8 T cells on day 6 of culture days, were cultured
833 in fresh warm complete medium and cytokine for 2 hours before cells were harvested,
834 washed twice in ice-cold HBSS and cell pellets snap frozen in liquid nitrogen. Duplicate cell
835 pellets were collected per sample for parallel processing for proteomics or RNAseq analysis.
836
837 IL-2 expanded P14 CD8 T cells on day 5 of culture were treated for 24 hours with PIM447 (5
838 µM) or AZD1208 (10 µM). Cells were harvested on day 6 of culture, washed twice in ice-cold
839 HBSS and cell pellets snap frozen in liquid nitrogen.
840
841 For all proteomics samples, cell pellets were lysed in 4% SDS, 50 mM TEAB pH 8.5, 10 mM
842 TCEP (5 min, 1200 rpm, room temperature), boiled (5 min, 500 rpm, 95 ^{o}C), then sonicated
843 with a BioRuptor (30 s on, 30 s off x30 cycles). Protein concentration was determined using
844 EZQ protein quantitation kit (Invitrogen) as per manufacturer instructions. Lysates were
845 alkylated with 20 mM iodoacetamide (Sigma) for 1 hours at room temperature in the dark.

846 24 hour TCR WT and Pim dKO CD4 and CD8 T cell proteomics samples and Day 6, 24 hour
847 pan-PIM kinase inhibitor treated IL-2 expanded CD8 T cell samples were cleaned up and
848 peptides generated by an SP3 bead protocol (Hughes et al., 2014) as described previously
849 (Marchingo et al., 2020). As outlined in reference (Marchingo et al., 2020): "Briefly, 200 µg
850 of 1:1 mixed Hydrophobic and Hydrophilic Sera-Mag SpeedBead Carboxylate-Modified
851 Magnetic Particles were added per protein sample then acidified to ~pH 2.0 by addition 10:1
852 Acetonitrile: Formic Acid. Beads were immobilised on a magnetic rack and proteins washed
853 with 2 × 70% ethanol and 1 × 100% acetonitrile. Rinsed beads were reconstituted in 0.1%
854 SDS 50 mM TEAB pH 8.5, 1 mM CaCl2 and digested overnight with LysC followed by
855 overnight digestion with Trypsin, each at a 1:50 enzyme to protein ratio. Peptide clean up
856 was performed as per SP3 procedure (Hughes et al., 2014). Briefly, protein-bead mixtures
857 were resuspended and 100% acetonitrile added for 10 min (for the last 2 min of this beads
858 were immobilised on a magnetic rack). Acetonitrile and digest buffer were removed,
859 peptides were washed with acetonitrile and eluted in 2% DMSO. Peptide concentration was
860 quantified using CBQCA protein quantitation kit (Invitrogen) as per manufacturer protocol.
861 Formic acid was added to 5% final concentration".
862
863 24 hour TCR WT and Pim dKO CD4 and CD8 T cell proteomics samples were fractionated
864 using high pH reverse phase liquid chromatography as described previously (Marchingo et
865 al., 2020). As outlined in reference (Marchingo et al., 2020): "Samples were loaded onto a
866 2.1 mm x 150 mm XBridge Peptide BEH C18 column with 3.5 µm particles (Waters). Using a
867 Dionex Ultimate3000 system, the samples were separated using a 25 min multistep gradient
868 of solvents A (10 mM formate at pH 9 in 2% acetonitrile) and B (10 mM ammonium formate
869 pH 9 in 80% acetonitrile), at a flow rate of 0.3 mL/min. Peptides were separated into 16
870 fractions which were consolidated into eight fractions. Fractionated peptides were dried in
871 vacuo then dissolved in 5% Formic Acid for analysis by LC-ES-MS/MS".
872 24 hour pan-PIM kinase inhibitor treated day 6 IL-2 expanded CD8 T cell samples, were not
873 fractionated. They were dried in vacuo then dissolved in 5% Formic Acid for analysis by LC-
874 ES-MS/MS after SP3 cleanup.
875
876 Day 6 IL-2 and IL-15 expanded WT and PimdKO CD8 T cells samples were cleaned up and
877 peptides generated by an S-Trap protocol (Zougman et al., 2014) as per manufacturer

878 protocol (Protifi). Briefly, add phosphoric acid (to final concentration 1.2%) then S-Trap
879 binding buffer (90% methanol, 100 mM TEAB, pH 7.1) at a ratio 1:7 v:v lysate:binding buffer
880 was added to sample lysates containing 100-300 µg total protein. Acidified lysates were
881 loaded to S-Trap mini columns and spun (4,000 g, 30 s) until all SDS lysate/S-Trap buffer had
882 passed through the column. Proteins were digested on column in digest buffer (50 mM
883 sodium bicarbonate) containing Trypsin at a 1:20 enzyme to protein ratio (2 hours, 47°C
884 without shaking). Peptides were eluted by spinning in digest buffer (1000g, 1 min), then
885 0.2% aqueous formic acid (1000g, 1 min), then 50% acetonitrile 0.2% formic acid (4000g, 1
886 min). Peptide concentration was quantified using CBQCA protein quantitation kit
887 (Invitrogen) as per manufacturer protocol. Peptides were dried in vacuo then dissolved in
888 5% Formic Acid for analysis by LC-ES-MS/MS.
889
890 **Liquid chromatography electrospray tandem mass spectrometry analysis (LC-ES-MS/MS)**
891 ≤1 µg of peptide was analysed per fraction by Data-Dependent Acquisition (DDA) Mass
892 Spectrometry for 24 hour TCR WT and Pim dKO CD4 and CD8 T cell proteomics samples.
893 For label-free DDA proteomics of WT and Pim dKO CD4 and CD8 24 hour TCR activated T
894 cells samples were analysed as described previously (Sinclair et al., 2019). As outlined in
895 reference (Sinclair et al., 2019): "samples were injected onto a nanoscale C18 reverse-phase
896 chromatography system (UltiMate 3000 RSLC nano, Thermo Scientific) then electrosprayed
897 into an Orbitrap mass spectrometer (LTQ Orbitrap Velos Pro; Thermo Scientific). For
898 chromatography buffers were as follows: HPLC buffer A (0.1% formic acid), HPLC buffer B
899 (80% acetonitrile and 0.08% formic acid) and HPLC buffer C (0.1% formic acid). Peptides
900 were loaded onto an Acclaim PepMap100 nanoViper C18 trap column (100 µm inner
901 diameter, 2 cm; Thermo Scientific) in HPLC buffer C with a constant flow of 10 µl/min. After
902 trap enrichment, peptides were eluted onto an EASY-Spray PepMap RSLC nanoViper, C18, 2
903 µm, 100 Å column (75 µm, 50 cm; Thermo Scientific) using the buffer gradient: 2% B (0 to 6
904 min), 2% to 35% B (6 to 130 min), 35% to 98% B (130 to 132 min), 98% B (132 to 152 min),
905 98% to 2% B (152 to 153 min), and equilibrated in 2% B (153 to 170 min) at a flow rate of 0.3
906 µl/min. The eluting peptide solution was automatically electrosprayed using an EASY-Spray
907 nanoelectrospray ion source at 50° and a source voltage of 1.9 kV (Thermo Scientific) into
908 the Orbitrap mass spectrometer (LTQ Orbitrap Velos Pro; Thermo Scientific). The mass
909 spectrometer was operated in positive ion mode. Full-scan MS survey spectra (mass/charge

910 ratio, 335 to 1800) in profile mode were acquired in the Orbitrap with a resolution of
911 60,000. Data were collected using data- dependent acquisition: the 15 most intense peptide
912 ions from the preview scan in the Orbitrap were fragmented by collision-induced
913 dissociation (normalized collision energy, 35%; activation Q, 0.250; activation time, 10 ms) in
914 the LTQ after the accumulation of 5000 ions. Precursor ion charge state screening was
915 enabled, and all unassigned charge states as well as singly charged species were rejected.
916 The lock mass option was enabled for survey scans to improve mass accuracy. (Using Lock
917 Mass of 445.120024)".
918
919 ~0.2 µg of peptide was analysed per sample by single shot DDA Mass Spectrometry for 24
920 hour pan-PIM kinase inhibitor treated, day 6 IL-2 expanded CD8 T cell samples.
921 Samples were injected onto a nanoscale C18 reverse-phase chromatography system
922 (UltiMate 3000 RSLC nano, Thermo Scientific) then electrosprayed into a Q-Exactive HF
923 (Thermo Scientific). A 2- 35% B gradient comprising of eluent A (0.1% formic acid) and
924 eluent B (80% acetonitrile/0.1% formic acid) was used to run a 120-minute gradient per
925 sample. With the mass spectrometer in positive mode the top 20 most intense peaks from a
926 mass range of 335-1800 m/z in each MS1 scan with a resolution of 60,000 were then taken
927 for MS2 analysis at a resolution of 15,000. Spectra were fragmented using Higher-energy C-
928 trap dissociation (HCD).
929
930 2 µg of peptide was analysed per sample by Data-Independent Acquisition (DIA) Mass
931 Spectrometry for the IL-2 and IL-15 expanded CD8 T cell proteomics samples. For label-free
932 DIA proteomics of Day 6 IL-2 and IL-15 expanded WT and Pim dKO CD8 T cells peptide samples
933 were analysed as described in (Sollberger et al., 2023) with some minor differences. Peptides
934 were injected onto a nanoscale C18 reverse-phase chromatography system (UltiMate 3000
935 RSLC nano, Thermo Scientific) then electrosprayed into an Orbitrap Exploris 480 Mass
936 Spectrometer (Thermo Scientific). For liquid chromatography buffers were as follows: buffer
937 A (0.1% formic acid in Milli-Q water (v/v)) and buffer B (80% acetonitrile and 0.1% formic acid
938 in Milli-Q water (v/v). Sample were loaded at 10 µL/min onto a trap column (100 µm × 2 cm,
939 PepMap nanoViper C18 column, 5 µm, 100 Å, Thermo Scientific) equilibrated in 0.1%
940 trifluoroacetic acid (TFA). The trap column was washed for 3 min at the same flow rate with
941 0.1% TFA then switched in-line with a Thermo Scientific, resolving C18 column (75 µm × 50

942 cm, PepMap RSLC C18 column, 2 µm, 100 Å). The peptides were eluted from the column at a
943 constant flow rate of 300 nl/min with a linear gradient from 3% buffer B to 6% buffer B in 5
944 min, then from 6% buffer B to 35% buffer B in 115 min, and finally to 80% buffer B within 7
945 min. The column was then washed with 80% buffer B for 4 min and re-equilibrated in 3%
946 buffer B for 15 min. Two blanks were run between each sample to reduce carry-over. The
947 column was kept at a constant temperature of 40°C.
948 The data was acquired using an easy spray source operated in positive mode with spray
949 voltage at 2.1 kV and the ion transfer tube temperature at 275°C. The MS was operated in
950 DIA mode. A scan cycle comprised a full MS scan (m/z range from 350-1650, with RF lens at
951 40%, AGC target set to custom, normalised AGC target at 300%, maximum injection time
952 mode set to custom, a maximum ion injection time of 20 ms, microscan set to 1 and source
953 fragmentation disabled. MS survey scan was followed by MS/MS DIA scan events using the
954 following parameters: multiplex ions set to false, collision energy mode set to stepped,
955 collision energy type set to normalized, HCD collision energies set to 25.5, 27 and 30%,
956 orbitrap resolution 30000, first mass 200, RF lens 40%, AGC target set to custom, normalized
957 AGC target 3000%, microscan set to 1 and maximum injection time 55 ms. Data for both MS
958 scan and MS/MS DIA scan events were acquired in profile mode.
959
960 **Proteomics data analysis**
961 The 24 hour TCR WT and Pim dKO CD4 and CD8 T cell DDA proteomics data and 24 hour
962 pan-PIM kinase inhibitor treated Day 6 IL-2 expanded CD8 T cell DDA proteomics data were
963 processed, searched and quantified with the MaxQuant software package, version
964 1.6.10.43. For the protein and peptide searches we generated a hybrid database consisting
965 of all manually annotated mouse SwissProt entries, combined with mouse TrEMBL entries
966 with protein level evidence available and a manually annotated homologue within the
967 human SwissProt database as described in (Marchingo et al., 2020). For the 24 hour TCR
968 activated data this was from the Uniprot release 2020_06, for the 24 hour PIM kinase
969 inhibitor data this was from the Uniprot release 2019_08. Search parameters were as
970 described in (Marchingo et al., 2020): "The following MaxQuant search parameters were
971 used: protein N-terminal acetylation, methionine oxidation, glutamine to pyroglutamate,
972 and glutamine and asparagine deamidation were set as variable modifications and
973 carbamidomethylation of cysteine residues was selected as a fixed modification; Trypsin and

974 LysC were selected as the enzymes with up to two missed cleavages permitted; the protein
975 and PSM false discovery rate was set to 1%; matching of peptides between runs was
976 switched off".
977 Data filtering and protein copy number quantification was performed in the Perseus
978 software package, version 1.6.6.0. Proteins were quantified from unique peptides and razor
979 peptides (peptides assigned to a group, but not unique to that group). The data set was
980 filtered to remove proteins categorised as 'contaminants', 'reverse' and 'only identified by
981 site'.
982 To generate a point of reference between TCR activated WT and Pim dKO and inactive T
983 cells, naïve WT CD4 and CD8 T cell data from (Marchingo et al., 2020), which was collected
984 and processed identically, was included in proteomics search, results table and plot of
985 protein content. At this point biological replicate 3 from Pim dKO CD4 T cells was excluded
986 from further analysis due to poor sample quality (e.g. protein sequence coverage was an
987 average of 13.9% compared to an average of 18.2-24.6% for all other samples and
988 estimated total protein content per cell was ~1/3rd of that observed in the other two
989 biological replicates for that condition, despite no obvious difference in FSC measured when
990 FACS sorting).
991
992 The day 6 IL-2 and IL-15 expanded WT and Pim dKO CD8 T cell DIA proteomics data files were
993 searched using Spectronaut version 14.7. Data was analysed using a library-free approach.
994 Raw proteomics data files were searched using the Pulsar tool within Spectronaut using the
995 following settings: 0.01 FDR at the protein and peptide level with digest rule set to 'Trypsin'P'.
996 A maximum of two missed cleavages and minimum peptide length of 7 amino acids was
997 selected. Carbamidomethyl of cysteine was selected as a fixed modification while protein n-
998 terminal acetylation and methionine oxidation were selected as variable modifications.
999 Manufacturer default settings were used for identification, with protein and precursor q-
1000 value set to 0.01 using default decoy strategy. For quantification settings, the MS-Level
1001 quantity was set to 'MS2', major group Top N and minor group Top N were set as 'False' and
1002 profiling was set as 'False'. The data was searched against the same mouse Uniprot database
1003 as used above for DDA analysis.
1004

1005 Data was filtered to only include proteins for which at least one condition had peptides
1006 detected in ≥2 biological replicates for 24 hour TCR and day 6 IL-2 and IL-15 WT and Pim
1007 dKO data. Data was filtered to only include proteins for which at least two conditions had
1008 peptides detected in ≥2 biological replicates for PIM kinase inhibitor data. Mean copy
1009 number per cell was calculated using the 'proteomic ruler' plugin as described in
1010 (Wisniewski et al., 2014).
1011 Mass contribution of proteins (g/cell) was calculated as (protein copy number) * (molecular
1012 weight (Daltons)) / (Avogadro's constant). Differential expression analysis of protein copy
1013 number was performed using RStudio (version 1.2.5033). P-values and fold-change were
1014 calculated with the Bioconductor package Limma (version 3.44.3). Q-values were calculated
1015 using Bioconductor package qvalue (version 2.20.0).
1016
1017 All scripts used to perform analysis are available from authors upon request.
1018
1019 **RNAseq:**
1020 **RNA extraction and library preparation and RNA sequencing:**
1021 Biological triplicate cell pellets of day 6 IL-2 or IL-15 differentiated CD8 T cells were collected
1022 in parallel with proteomics samples as described above. Total RNA was extracted from cell
1023 pellets with Qiagen RNAeasy mini kit (Qiagen) as per manufacturer instructions.
1024 2 µg of RNA was submitted per sample to the Finnish Functional Genomics Centre, University
1025 of Turku and Åbo Akademi University for library preparation and sequencing. RNA quality was
1026 verified using Agilent Bioanalyzer 2100 or Advanced Analytical Fragment Analyzer. 300 ng of
1027 total RNA was used for library preparation using the Illumina TruSeq Stranded mRNA sample
1028 preparation kit (15031047) as per manufacturer instructions. Library quality was confirmed
1029 with Advanced Analytical Fragment Analyzer and quantified with Qubit Fluorometric
1030 Quantitation (Life Technologies). Sample libraries were pooled and run in a single lane on an
1031 Illumina NovaSeq 6000 with read length 2x 50 bp. Base calling was performed with bcl2fastq2
1032 conversion software (NovaSeq 6000) and automatic adapter trimming performed for fastq
1033 raw read files generated.
1034
1035
1036

1037 **RNAseq data analysis**

1038 Quality assessment of raw reads was evaluated using MultiQC (Ewels et al., 2016). Raw reads
1039 were aligned to the GRCm38.p6 (Ensembl) build of the Mus musculus reference genome using
1040 the STAR aligner (Dobin et al., 2013) (version 2.7.1a), with 'outFilterType BySJout' option
1041 switched on to reduce spurious junctions. The STAR quantMode GeneCounts option was used
1042 to map aligned reads to genes to generate a gene counts matrix, using the annotation file
1043 GRCm38.101 (Ensembl).

1044

1045 Bioconductor package EdgeR (version 3.30.3) (Robinson et al., 2010; McCarthy et al., 2012)
1046 was used to reduce noise from low count genes with filterByExpr function and the resulting
1047 count matrix was normalised by the EdgeR Trimmed Mean of M-values (TMM) method.
1048 Differential expression analysis was performed using Limma package (version 3.44.3) (Ritchie
1049 et al., 2015; Law et al., 2016). Reads were converted to $\log_2$ counts per million and weighted
1050 using the voomWithQualityWeights function. A linear model was fitted to each gene and
1051 empirical Bayes moderated t-statistics were applied. q-values were calculated from using
1052 Bioconductor package qvalue (version 2.20.0) (Storey et al., 2023). The calculateTPM fuction
1053 from the Bioconductor package Scater (version 1.16.2) (McCarthy et al., 2017) was used to
1054 calculate TPM values for visualisation purposes, with total exon length calculated using
1055 GenomicRanges (version 1.40.0) (Lawrence et al., 2013) as the sum of the non-overlapping
1056 exonic regions for a gene.

1057

1058 **Combining Proteomics and RNAseq data**

1059 Proteomics data was annotated during Spectronaut search and Perseus analysis with Uniprot
1060 ID, MGI symbol and MGI ID information. BioMart (version 2.47.2) was used to extract UniProt
1061 identifiers, MGI symbols and MGI IDs for corresponding ENMUSG IDs of RNAseq data. RNAseq
1062 data was first combined with proteomics data based on UniProt ID. Proteins that didn't
1063 receive an initial match, were then combined by matching MGI ID values, then if still
1064 unmatched by MGI symbol. Data combinations were manually checked for obvious mis-
1065 annotations. Proteins with no corresponding mRNA identified or vice versa were excluded
1066 from the combined data file. In a few instances multiple proteins aligned to a single mRNA
1067 measurement or multiple mRNA aligned to a single protein measurement. For the purposes

1068 of this broad examination of how differences in expression at the protein or mRNA level these
1069 results were also excluded from the combined data table and subsequent analysis.
1070
1071 **Graphing and statistics**
1072 Heatmaps were generated using Broad Institute software Morpheus
1073 (https://software.broadinstitute.org/morpheus). Statistical tests performed for experiments
1074 other than proteomics and RNAseq are indicated in figure legends and were performed in
1075 Prism (GraphPad, version 9 or 10).
1076
1077 **Data availability**
1078 All data generated or analysed during this study are included in the manuscript and
1079 supporting files. Raw mass spec data files and MaxQuant or Spectronaut analysis files are
1080 available on the ProteomeXchange data repository and can be accessed with the following
1081 identifiers: PXD051198 for 24 hour TCR activated WT and Pim dKO CD4 and CD8 T cells;
1082 Naïve T cell data used as a point of reference for plotting 24 hour TCR proteomics has
1083 previously been published as part of (Marchingo et al., 2020) and can also be found under
1084 the identifier PXD016105; PXD051214 for Pim inhibitor proteomics; PXD051213 for day 6 IL-
1085 2 and IL-15 expanded WT and Pim dKO CD8 T cells. An easy-to-use graphical interface for
1086 examining protein copy number expression from the 24-hour TCR WT and Pim dKO CD4 and
1087 CD8 T cell proteomics and IL-2 and IL-15 expanded WT and Pim dKO CD8 T cell proteomics
1088 datasets is also available on the Immunological Proteome Resource website: immpres.co.uk
1089 (Brenes et al., 2023) under the Cell type(s) selection: “T cell specific” and Dataset selection:
1090 “Pim1/2 regulated TCR proteomes” and “Pim1/2 regulated IL2 or IL15 CD8 T cell
1091 proteomes”. Raw RNAseq data files are available on the NCBI GEO website and can be
1092 accessed with the identifier GSE261667.

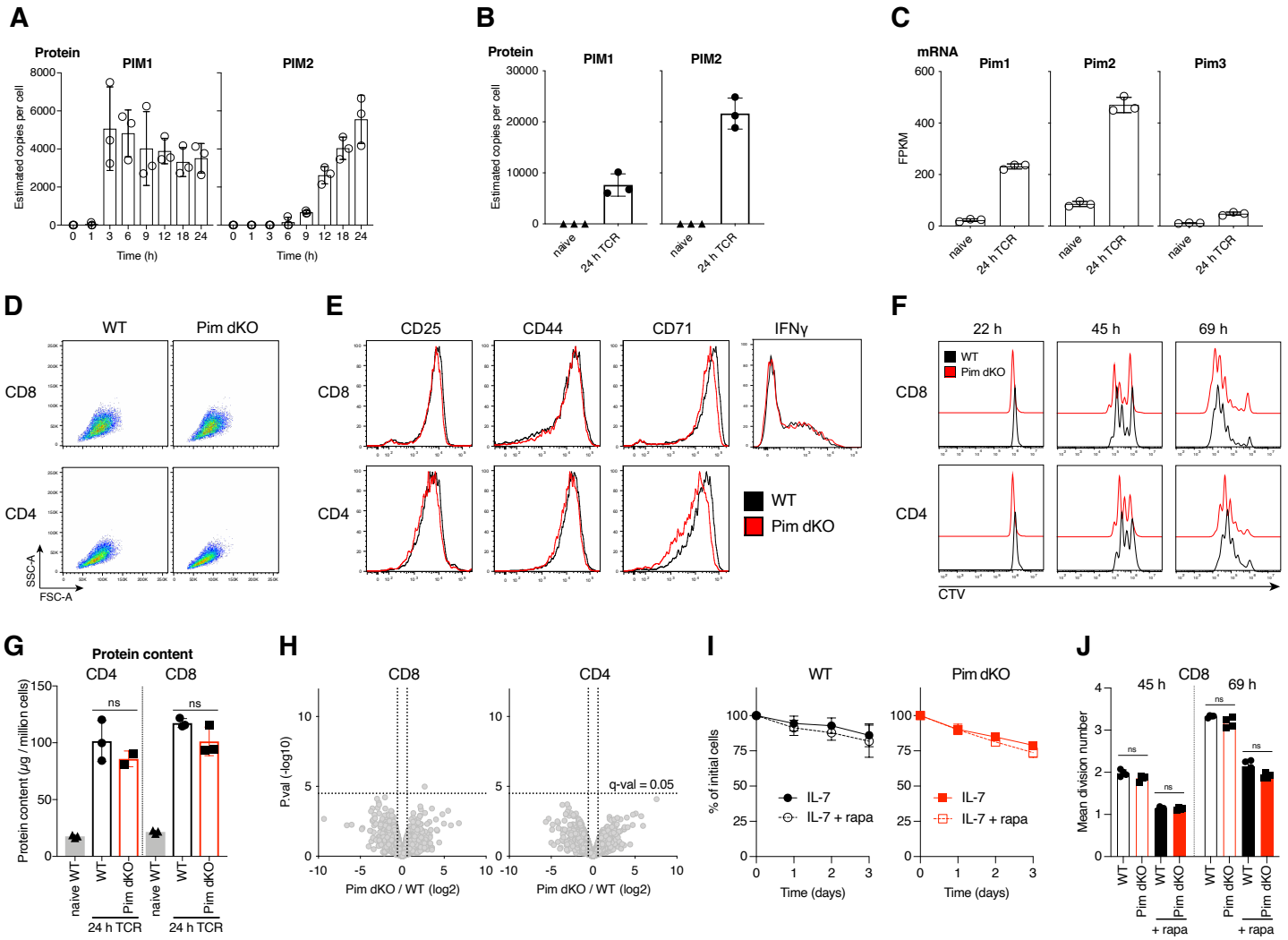

Figure 1. Pim1 and Pim2 are strongly TCR-induced, but dispensable for T cell activation

Estimated copies per cell of PIM1 and PIM2 protein from quantitative proteomics analysis of (**A**) OT1 CD8 T cells stimulated with SIINFEKL peptide for indicated times from published dataset (Marchingo et al., 2020) or (**B**) naïve ex vivo and 24 hour αCD3/αCD28 (TCR) activated WT CD8 T cells (see Fig 1G-H) for further details. (**C**) Fragments per kilobase million (FPKM) of *Pim1*, *Pim2* and *Pim3* mRNA from published (Spinelli et al., 2021) bulk RNAseq analysis of naïve and 24 hour gp33-41 peptide stimulated P14 CD8 T cells. Lymph node cell suspensions from C57BL/6 (WT) and *Pim1*KO/*Pim2*KO (Pim dKO) mice were activated for 24 hours with αCD3/αCD28 (both 0.5 µg/mL) and CD4 and CD8 T cell (**D**) FSC-A SSC-A profiles, (**E**) expression of surface activation markers (CD25, CD44, CD71) or CD8 T cell intracellular IFNγ were measured by flow cytometry. (**F**) Lymph node single cell suspensions from WT and Pim dKO mice were labelled with CellTrace Violet (CTV), activated with αCD3/αCD28 (both 0.5 µg/mL) and CD4 and CD8 T cell CTV proliferation profiles were measured at indicated time points. (G-H) Lymph node cell suspensions from WT and Pim dKO mice were stimulated for 24 hours with αCD3/αCD28 (both 0.5 µg/mL) and activated CD4 and CD8 T cells were sorted for analysis by quantitative proteomics. Data was analysed using proteomic ruler method (Wisniewski et al., 2014) to estimate protein copy number per cell. An interactive version of the proteomics expression data is available for exploration on the Immunological Proteome Resource website: immpres.co.uk (**G**) Total protein content (µg/million cells) (one-way ANOVA), (**H**) Volcano plots of p-value ($-\log_{10}$) versus fold-change ($\log_2$) in protein copy number between Pim dKO and WT. Horizontal dotted line represents multi-test correction cut-off of q=0.05, vertical dotted line shows 1.5-fold change. Phosphoribosyl Pyrophosphate synthase 1 like 1 (Prps1l1), was found to be higher in Pim dKO CD8 T cells, but was a low confidence quantification (based on only 2 unique peptides) with no known function in T cells. Lymph node single cell suspensions from WT and Pim dKO mice were labelled with CellTrace Violet (CTV) and (**I**) cells were cultured in IL-7 (5ng/mL) +/- rapamycin (20 nM) and CD8 T cell numbers measured over time or (**J**) cells were activated with αCD3/αCD28 (both 0.5 µg/mL) +/- rapamycin (20 nM) and CD8 T cell mean division number was calculated over time (two-way ANOVA). Symbols in bar charts represent biological replicates, symbols in (I) represent the mean. Error bars show mean ± S.D. Flow cytometry dot plots and histograms are representative of (D-E) n = 3, except for IFNγ staining which is n=2 or show pooled data from (I) n=3-4 and (F, J) n=5 biological replicates, with data collected over at least 2 independent experiments. Quantitative proteomics was performed on biological triplicates.

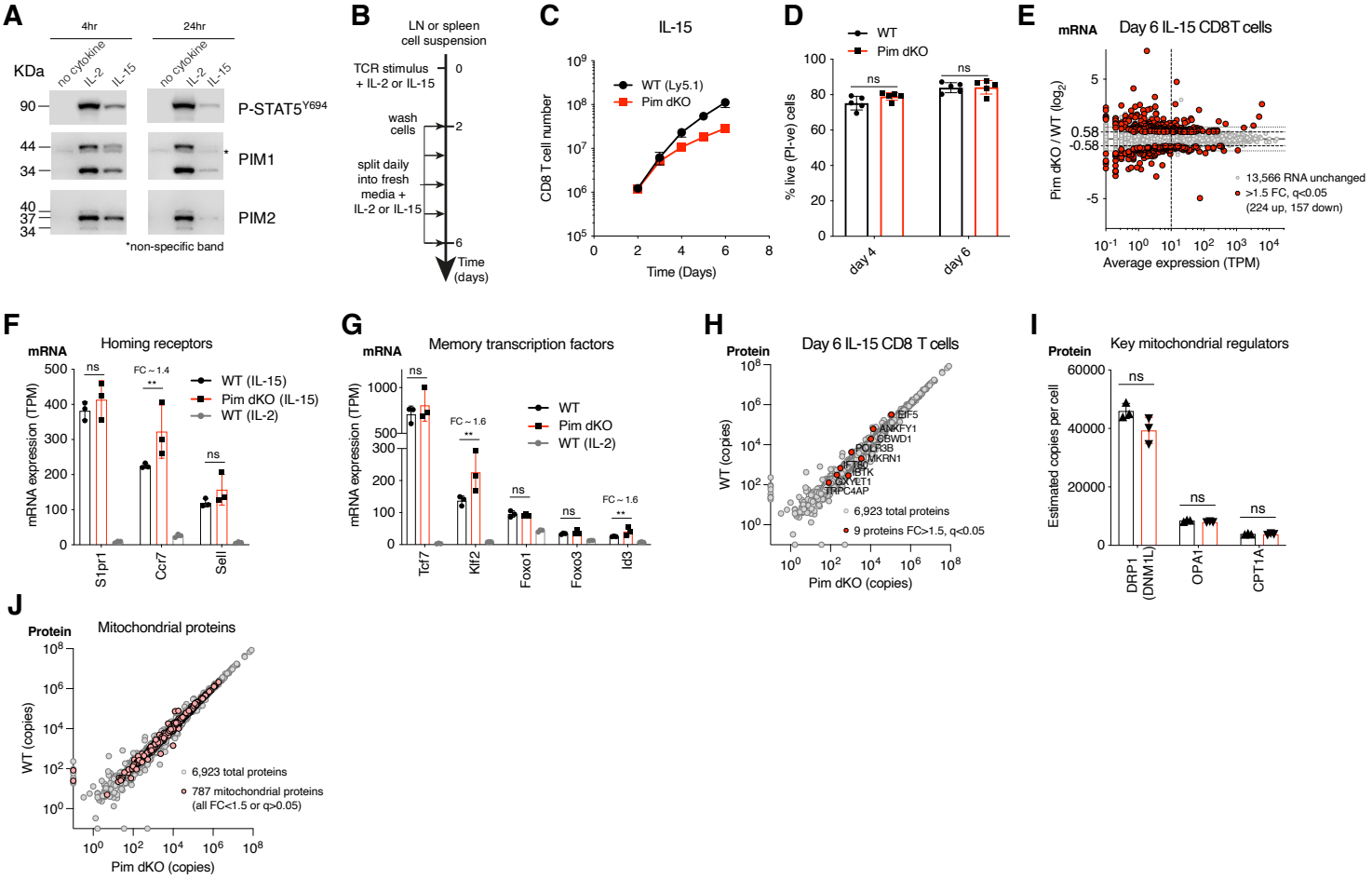

Figure 2. Pim1/Pim2 deficiency reduces IL-15-driven CD8 T cell proliferation but does not prevent memory differentiation.

(**A**) OT1 lymph node cell suspensions were SIINFEKL peptide activated for 36 hours, washed then cultured with no cytokine, IL-15 (20 ng/mL) or IL-2 (20 ng/mL) for 4 or 24 hours. Western blots of PIM1 (two isoforms of 44 and 34 kDa, non-specific band indicated by *), PIM2 (three isoforms of 40, 37 and 34 kDa) or pSTAT5 Y694 expression. (**B**) Schematic of cytokine driven memory and effector CD8 T cell expansion and differentiation cultures. Lymph node or spleen cell suspensions were activated for 2 days with TCR stimulus + cytokine, washed, then split daily into fresh media + cytokine. (**C**) WT (Ly5.1) and Pim dKO LN suspensions were mixed at a 50:50 ratio for T cells and cultured as outlined in (B) with TCR stimulus αCD3/αCD28 (both 0.5 µg/mL) + cytokine IL-15 (20 ng/mL), and CD8 T cell number was measured daily. (**D**) WT and Pim dKO T cells were expanded with IL-15 in separate cultures as per (B-C) and % live cells (PI-ve) were assessed on days 4 and 6 (two-way ANOVA). (E-J) WT and Pim dKO CD8 T cells were activated with TCR stimulus αCD3/αCD28 (both 0.5 µg/mL) + cytokine IL-15 (20 ng/mL), expanded with IL-15 as per (B), with an additional CD4 T cell magnetic depletion step on day 3 of culture. CD8 T cells were harvested on day 6 for parallel RNAseq and proteomic analysis. An interactive version of the proteomics expression data is available for exploration on the Immunological Proteome Resource website: immpres.co.uk (**E**) Fold-change in mRNA expression between Pim dKO and WT versus average mRNA expression (TPM). mRNA expression (Transcripts per million, TPM) of (**F**) secondary lymphoid homing receptors Sell, Ccr7, S1pr1 and (**G**) key transcription factors involved in CD8 T cell memory differentiation and maintenance Tcf7, Klf2, Foxo1, Foxo3, Id3. (**H**) WT vs Pim dKO protein copy numbers, differentially expression proteins (FC>1.5, q<0.05) are highlighted in red (**I**) Protein copy numbers per cell for key mitochondrial proteins DRP1, OPA1 and CPT1A. (**J**) WT vs Pim dKO protein copy numbers, mitochondrial proteins (as defined in MitoCarta 3.0) are highlight in pink. Symbols in bar charts represent biological replicates, symbols in (C,E,H,J) represent the mean. Error bars show mean ± S.D. Data are representative of (A) n=3 or show pooled data from (C) n = 4, and (D) n=5 biological replicates with data collected over at least 2 independent experiments. Quantitative proteomics and RNAseq was performed on biological triplicates. ** q≤0.01, fold-change (FC) shown on bar graphs when q<0.05.

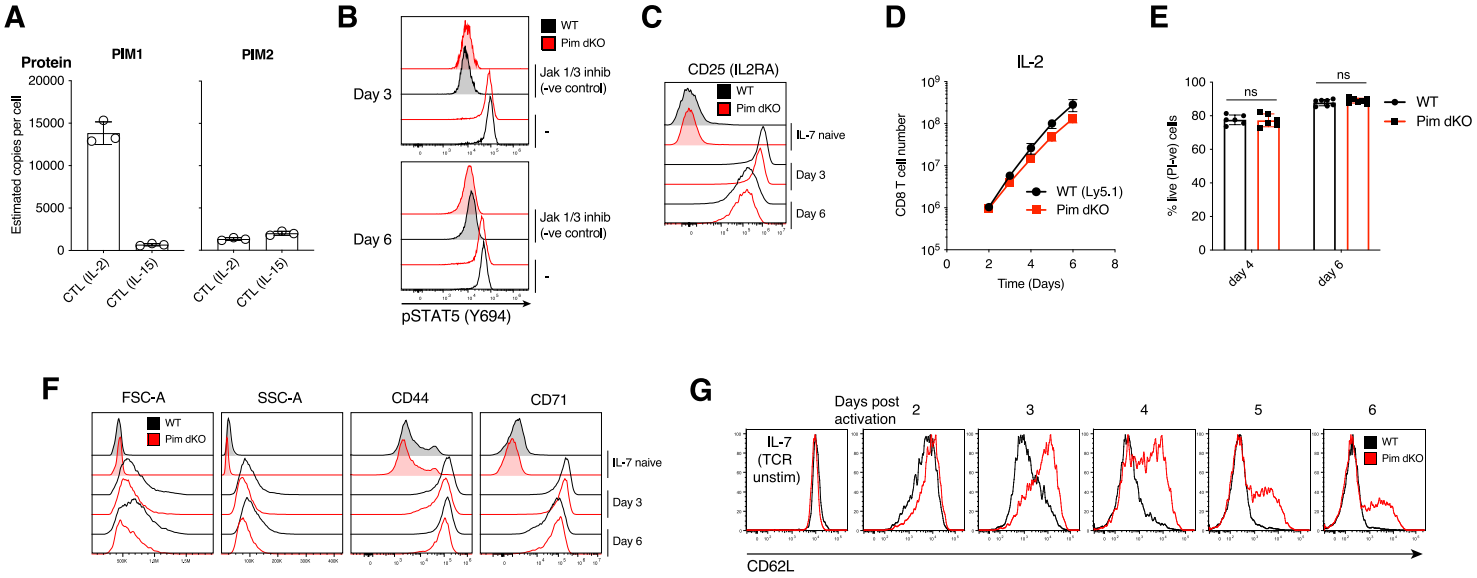

Figure 3. Pim dKO IL-2 differentiated effector T cells have reduced cell size and sustained expression of CD62L

(**A**) Estimated copies per cell of PIM1 and PIM2 protein from published quantitative proteomics analysis (Howden et al., 2019; Brenes et al., 2023) of CD8 T cells expanded in IL-2 or IL-15 as outlined in Fig 2B. (B-D, F-G) WT (Ly5.1) and Pim dKO lymph node or spleen single cell suspensions were mixed at a 50:50 ratio of T cells, activated for 2 days with αCD3/αCD28 (both 0.5 µg/mL) and IL-2 (20 ng/mL), washed then split into fresh medium containing IL-2 (20 ng/mL) daily (as per Fig 2B). Some of the mixed cell suspensions were also cultured in IL-7 (5 ng/mL) to sustain a naïve T cell reference. (**B**) WT and Pim dKO CTL were treated 1 hour +/- Jak1/3 inhibitor Tofacitinib (100 nM) (negative control) before pSTAT5 Y694 expression was measured on day 3 and 6 of culture, (**C**) surface CD25 expression was measured on days 3 and 6 or culture, (**D**) CD8 T cell number vs time was calculated, (**F**) CD8 T cell FSC-A, SSC-A and surface activation markers (CD44, CD71) were measured on days 3 and 6 of culture (**G**) expression of adhesion molecule CD62L was measured daily. (**E**) WT and Pim dKO T cells were activated and expanded with IL-2 as per (Fig 3B-D, F-G) except in separate cultures and % live cells (PI-ve) was assessed on days 4 and 6 (two-way ANOVA).
Symbols in bar charts represent biological replicates, symbols in (D) represent the mean. Error bars show mean ± S.D. Data are representative of (B, G) n=4, (C,F) n=6 or show pooled data from (D) n=4, (E) n=6 biological replicates with data collected over at least 2 independent experiments

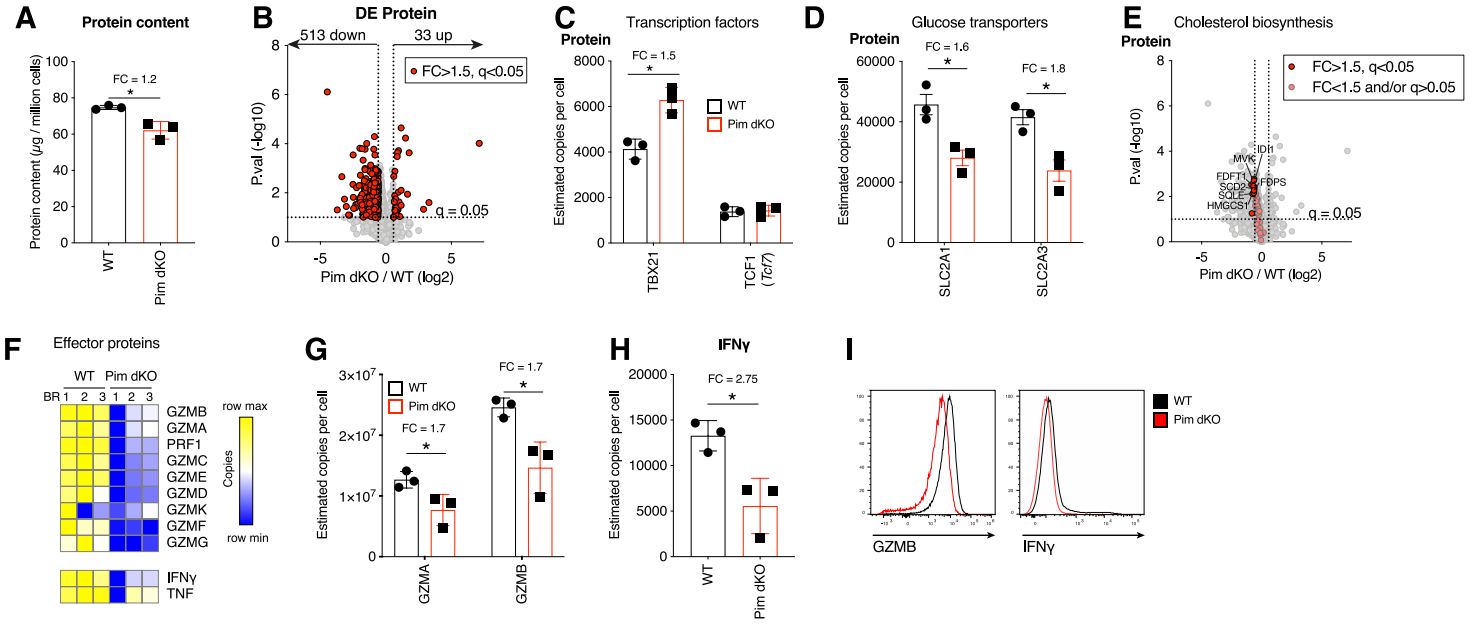

Figure 4. Major glucose transporters and effector proteins are reduced in Pim dKO IL-2 expanded CTL

WT and Pim dKO CD8 T cells were activated for 2 days with αCD3/αCD28 (both 0.5 µg/mL) and IL-2 (20 ng/mL), washed then split into fresh medium containing IL-2 (20 ng/mL) daily (as per Fig 2B), with an additional CD4 T cell magnetic depletion step on day 3 of culture. CD8 T cells were harvested on day 6 of culture for high resolution mass spectrometry. An interactive version of the proteomics expression data is available for exploration on the Immunological Proteome Resource website: immpres.co.uk (**A**) Estimated total protein content per cell (student t-test). (**B**) Volcano plots Pim dKO vs WT protein copy numbers, differentially expressed proteins (FC>1.5, q<0.05) are highlighted in red. Estimated protein copy number per cell of (**C**) transcription factor TBX21 and TCF1 (**D**) glucose transporters SLC2A1 and SLC2A3. (**E**) Volcano plots Pim dKO vs WT protein copy numbers. Proteins with KEGG term = "terpenoid backbone biosynthesis", "biosynthesis of unsaturated fatty acids" or "steroid biosynthesis" are highlighted with proteins with FC>1.5, q<0.05 shown in red and proteins with FC<1.5 and/or q>0.05 shown in pink. (**F**) Heatmap of protein copy numbers for granzymes, perforin and effector cytokines. Estimated protein copies for (**G**) major cytolytic Granzymes A and B and (**H**) IFNγ. (**I**) Granzyme B and IFNγ expression was measured by flow cytometry in day 6 IL-2 expanded WT and Pim dKO CTL.

Symbols in bar charts show biological replicates. Error bars show mean ± S.D. Data are representative of (G) n = 3-4, with data collected over at least 2 independent experiment Quantitative proteomics was performed on biological triplicates. * indicates q<0.05, fold-change (FC) shown on graph when q<0.05

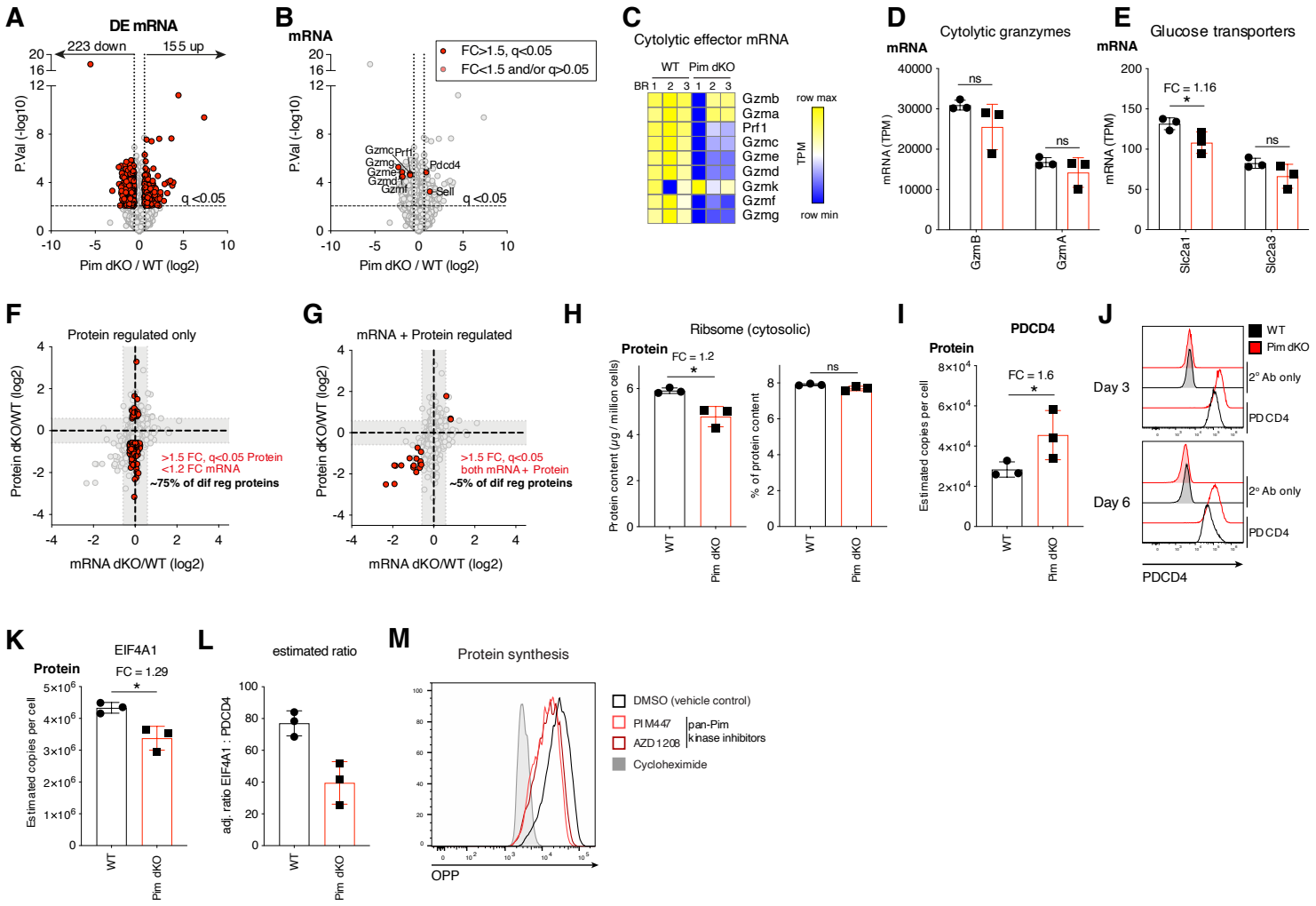

Figure 5. Disconnect between protein and mRNA expression in Pim1/Pim2-deficient effector CTL corresponds with a reduction in protein synthesis

RNAseq analysis was performed in day 6 IL-2 expanded WT and Pim dKO CD8 T cells which were collected in parallel with proteomics analysis described in Fig 4A. (**A**) Volcano plot of RNAseq data, differentially expressed mRNA (FC>1.5, q<0.05) are highlighted in red. (**B**) Volcano plot of RNAseq data, Granzymes C-K, perforin, Pdcd4 and Sell are highlighted in red. (**C**) Heatmap of mRNA expression (TPM) for granzymes, perforin and effector cytokines. Bar chart of mRNA expression (TPM) of (**D**) Granzymes A and B (**E**) Glucose transporters Slc2a1 and Slc2a3. (F-G) Fold change of PimdKO/WT protein (copies) from proteomics analysis described in Fig 4 vs mRNA (TPM) (**F**) highlighting in red proteins that are differentially expressed (FC>1.5, q<0.05) where mRNA is not substantially different (FC<1.2) and (**G**) highlighting in red protein and mRNA that are both differentially expressed (FC>1.5, q<0.05). (**H**) Estimated cytosolic ribosome content per cell (left), % ribosome of total cellular protein content (right). (**I**) Estimated protein copy number per cell of translation repressor PDCD4. (**J**) PDCD4 expression measured by flow cytometry on day 3 and 6 in IL-2 expanded WT vs Pim dKO CD8 T cells. (**K**) Estimated protein copy number per cell of EIF4A1. (**L**) adjusted ratio of PDCD4 : EIF4A1 (assuming 1 PDCD4 binds 2x EIF4A1) in WT and Pim dKO proteomes. (**M**) Protein synthesis measured by OPP incorporation in day 6 IL-2-expanded WT CTL treated for 24 hours with pan PIM kinase inhibitors PIM447 (5 µM) or AZD1208 (10 µM). 30 min cycloheximide (100 µg/mL) treatment gives no protein synthesis background control.

Symbols in bar charts show biological replicates: error bars show mean ± S.D. Data are representative of (M) n=2 biological replicates collected over two independent experiments, (J) n = 2 biological replicates. Quantitative proteomics and RNAseq were performed on biological triplicates. * indicates q<0.05, fold-change (FC) shown on graph when q<0.05.

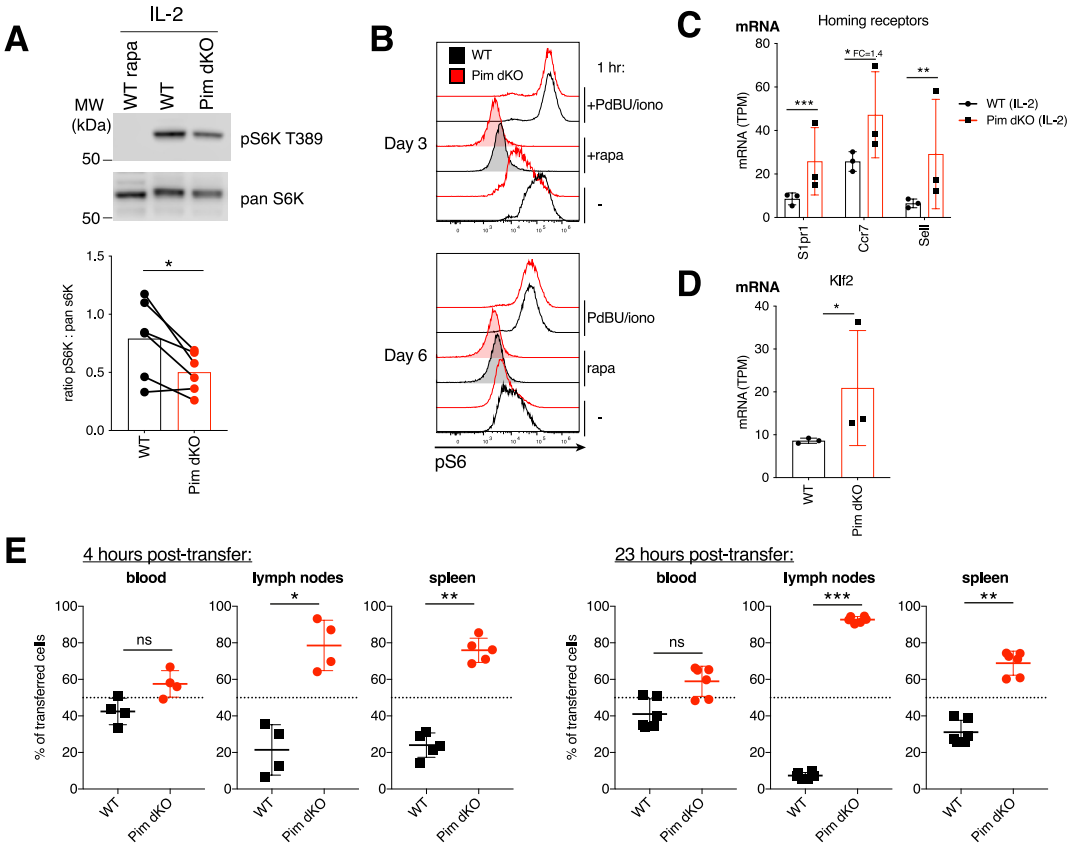

Figure 6. PIM kinases regulate mTORc1 activity and lymphoid homing in effector CTL

(**A**) Western blot of pS6K T389 and pan S6K from day 6 WT and PimdKO IL-2 CTL (paired student t-test, *= p<0.05). (**B**) WT and Pim dKO T cells were mixed in a 50:50 ratio, activated with αCD3/αCD28 (both 0.5 µg/mL) and IL-2 (20 ng/mL) and expanded in IL-2 as per Fig 2B and pS6 (Ser235/236) measured after 1 hr +/- PdBU and ionomycin (positive control), +/- rapamycin (mTORc1 inhibitor, negative control) or no additional treatment. mRNA expression (TPM) from RNAseq analysis of IL-2 expanded WT and Pim dKO CTL described in Fig 5A for (**C**) cell homing receptors S1pr1, Ccr7 and Sell and (**D**) transcription factor Klf2. (**E**) WT and Pim dKO T cells were activated and expanded with IL-2 in separate cultures as per Fig 2B. On day 6 of culture WT and Pim dKO CTL were labelled with CFSE or CTV, mixed at a 50:50 ratio and transferred into C57BL/6 recipient mice. Values indicate percentage of transferred cells detected in blood, lymph node or spleen 4 or 23 hours post-transfer that were WT or Pim dKO (one-way ANOVA).

Symbols show biological replicates. Error bars show mean ± S.D. Data are representative of (A) n= 6, (B) n=2-4 collected across at least 2 independent experiments and (E) n= 6 recipient mice, from n=2 biological donor replicates. RNAseq was performed on biological triplicates. * q<0.05, ** q<0.01, *** q<0.001, fold-change (FC) shown on graph when q<0.05 but FC<1.5.

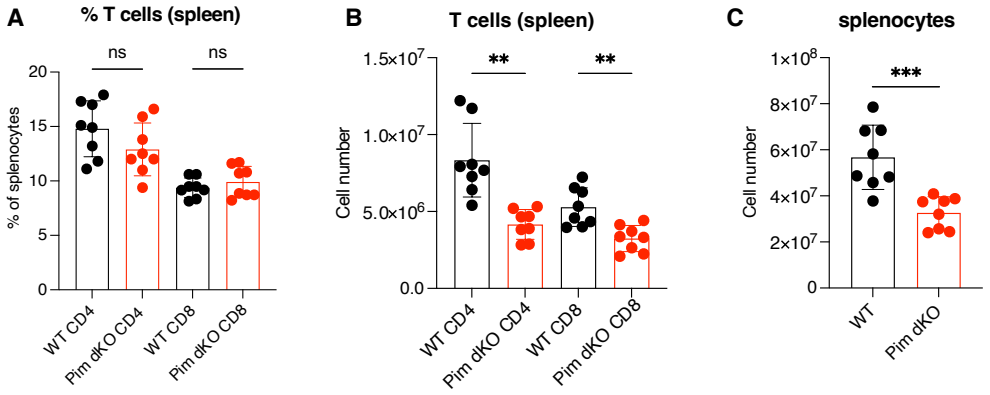

Figure S1. T cell counts in WT vs Pim dKO spleen

Comparison of Pim dKO and age/sex matched WT control mice for (**A**) proportion of splenocytes that were CD4+ and CD8+ (one-way ANOVA), (**B**) total number of CD4 and CD8 T cells in spleens (one-way ANOVA), and (**C**) total number of splenocytes (student t-test). Symbols in bar charts represent biological replicates: error bars show mean ± S.D. (A-C) n = 8 collected over 4 independent experiments. ** q<0.01, ***q<0.001.

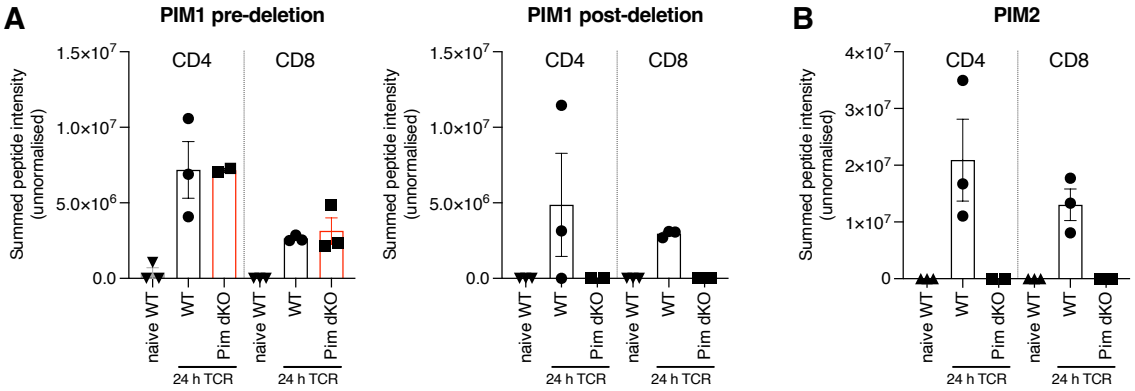

Figure S2. Proteomics data confirms deletion of catalytically active PIM1 and PIM2

Pim1 KO mice have the *Pim1* gene deleted from 98 codons post-ATG start site onwards (mid exon 4) and ablation of kinase activity was confirmed in (Laird et al., 1993). In Pim2 KO mice exons 1-3 are deleted from the *Pim2* gene (Mikkers et al., 2004). Summed peptide intensities from unnormalized proteomics data collected as described in Fig 1G-H from (**A**) before the PIM1 deletion point (left) and after the deletion point (right) and (**B**) whole of PIM2 protein confirms deletion of functional PIM1 and PIM2 protein.

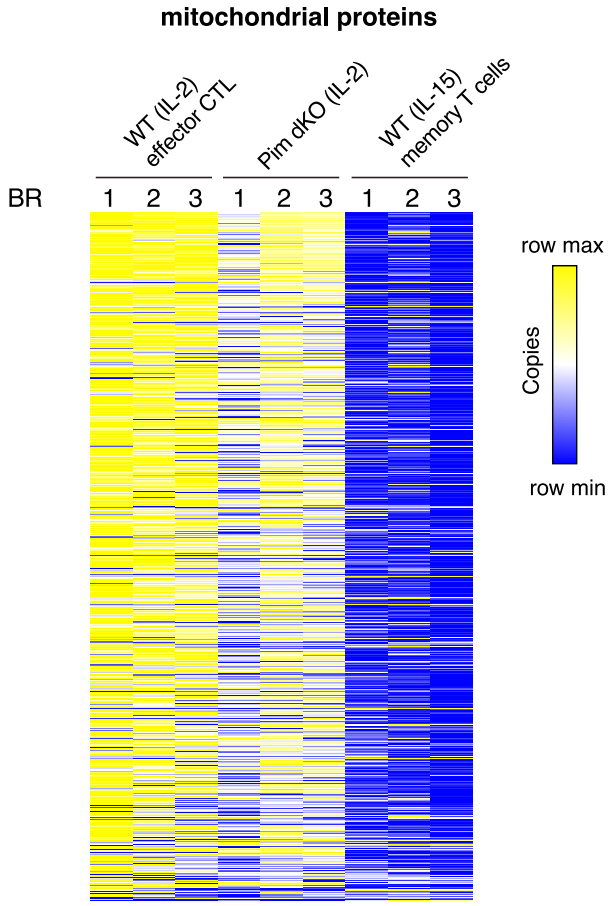

Figure S3. Pim dKO IL-2 expanded CD8 T cells exhibit an effector-like mitochondrial proteome profile

Heatmap showing protein copy number of mitochondrial proteins (as defined by inclusion on Mitocarta 3.0 list) from IL-2 expanded WT (effector), Pim dKO and IL-15 expanded WT (memory) proteomics experiments described in Fig 2 and 4. Proteins are ranked based on average expression in IL-2 WT condition. Proteomics was performed on biological triplicates.

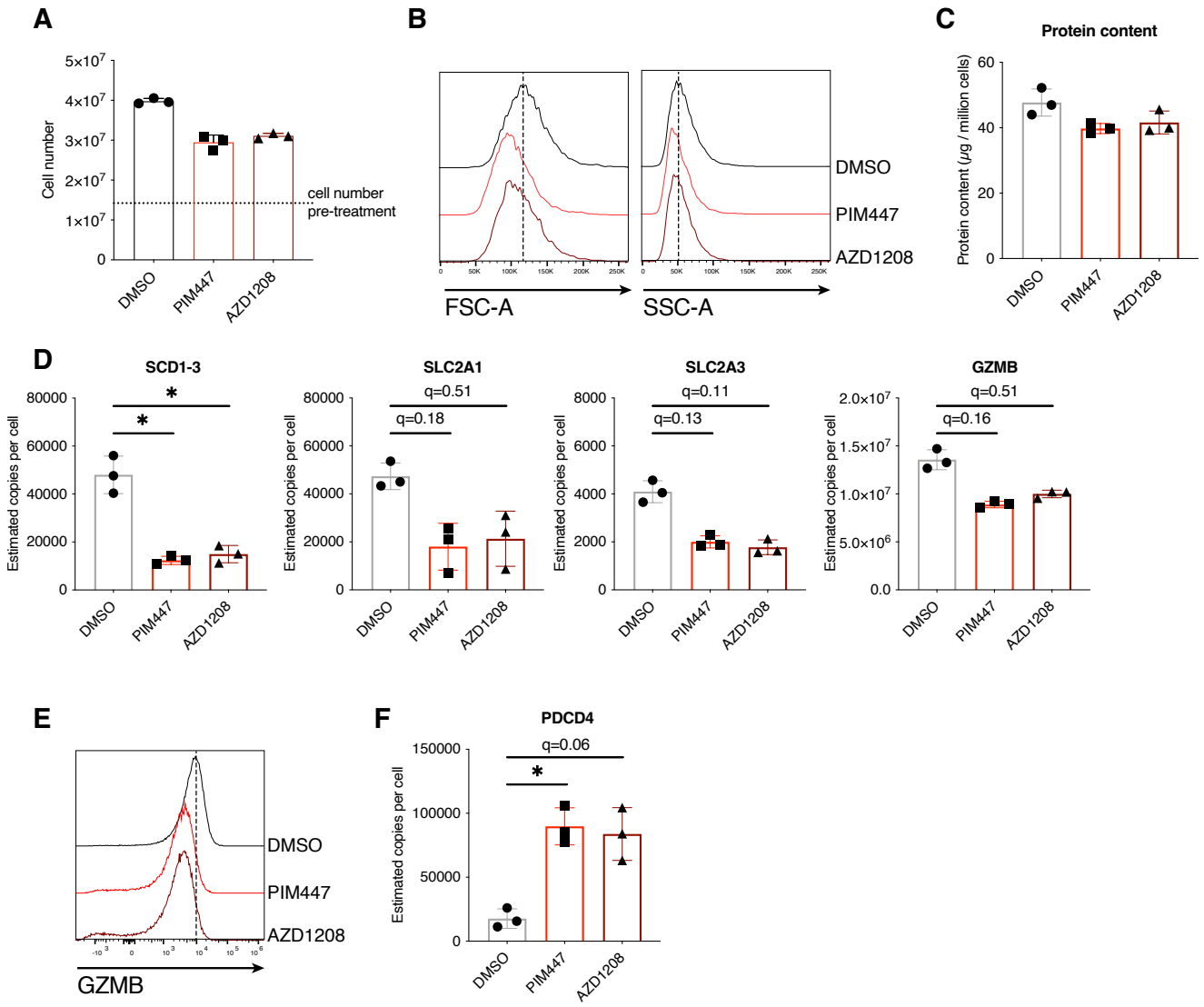

Figure S4. 24 hour treatment of IL-2 CTL with pan-PIM kinase inhibitors PIM447 or AZD1208 recapitulates many features of Pim1/Pim2-deficiency

Single cell suspension from P14 TCR-transgenic mouse lymph nodes were activated with gp33 peptide (100 ng/mL), IL-2 (20 ng/mL) and IL-12 (2 ng/mL) for 2 days, then split daily into fresh media containing IL-2 (20 ng/mL). On day 5 of culture IL-2 expanded CTL were treated with pan-PIM kinase inhibitors PIM447 (5 µM) or AZD1208 (10 µM) or DMSO vehicle control for 24 hours harvested on day 6 of culture to measure (**A**) Cell number (**B**) FSC-A SSC-A. Proteome analysis was also performed on inhibitor treated CTL to measure (**C**) protein content, (**D**) protein expression of SCD1-3, SLC2A1, SLC2A3, GZMB or (**F**) PDCD4. (**E**) Day 6 IL-2 expanded CTL from WT (C57BL/6) mice were treated for 24 hours with PIM447 or AZD1208 (both 1 µM) and GZMB expression was measured by flow cytometry.

Symbols show biological replicates. Error bars show mean ± S.D. Data are representative of (E) n=2 biological replicates collected across at least 2 independent experiments. Proteomics analysis was performed on biological triplicates, with (A-B) collected in parallel with proteomics analysis. * q<0.05.

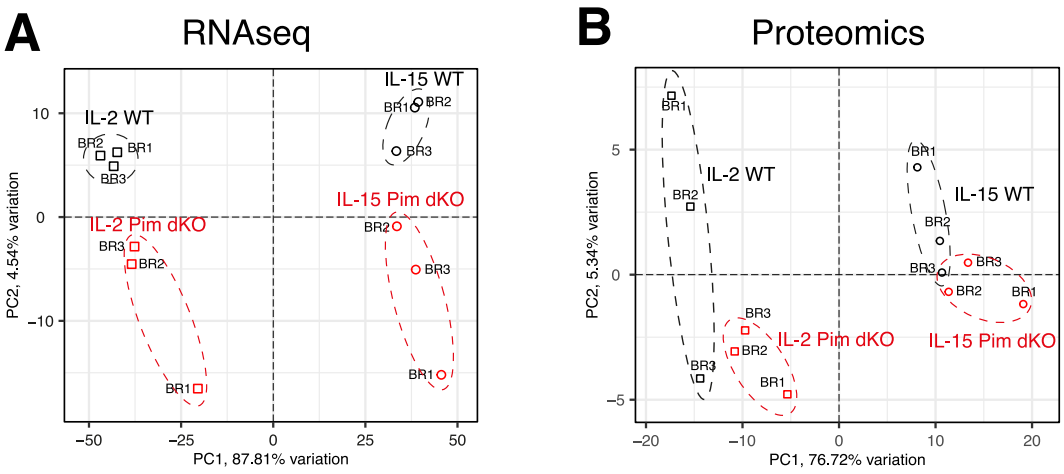

Figure S5. Pim dKO IL-2 expanded CD8 T cells are more similar to IL-2 WT effector T cells than IL-15 expanded memory T cells.

PCA plots from parallel (**A**) RNAseq and (**B**) proteomics analysis from Day 6 IL-2 and IL-15 expanded WT and Pim dKO CD8 T cells (as described in Fig 2, 4 and 5).